measured on a computer [10, 16].

Experimental protocol. After anesthesia, the catheter for injection of the contrast material was placed just above the bifurcation of the common iliac artery from the abdominal aorta via the right femoral artery. The rat was fixed on the acrylic board (5.0 mm thick) in standing position for angiography. Arterial pressure was monitored continuously by the catheter placed at the femoral artery, except during the period of the contrast material injection. The arterial systolic pressure ranged from 120 to 140 mmHg throughout the experimental period.

Sequential images of caudal arteries in the proximal portion of the tail were obtained by the injection of non-ionic contrast material (3 ml/s for 1 s, Iopamidol, Nihon Schering, Tokyo, Japan) via the arterial catheter. The contrast materials were infused twice, before and after the body temperature was increased from 37 to 39°C, by heating the body for 15 min using a hair-dryer. Body temperature was monitored using a thermometer (52 K/J Thermometer, Fluke, USA) inserted 6 cm into the rectum. The second angiography was performed 20 min after the first angiography. After completion of the angiographies, histological analysis (hematoxylin and eosin staining) of the tail was performed. The results of the second angiography were independent of the first. This was confirmed by preliminary experiments which indicated that the diameter change of the medial caudal artery was negligible 15 min after the contrast material injection (from 317±64 to 331±70 μm at 37°C, $n=5$, $p=0.739$; from 956±203 to 899±124 μm at 39°C, $n=5$, $p=0.553$).

All data obtained in the present study are expressed as means±SD. We applied a paired t-test for comparison of the mean values. Differences were considered significant at $p<0.05$.

RESULTS

The representative synchrotron radiation microangiographic images before and after the increase in body temperature are shown in Fig. 2. The large dumbbell-like structures in the center represent caudal vertebrae. The medial caudal artery (large arrows), the lateral caudal arteries (small arrows), and segmental anastomosing vessels (arrowheads) were visualized before heating. After heating, the medial caudal artery was markedly dilated (320±53 to 853±243 μm in diameter, $p<0.001$), while no significant change was observed in the lateral caudal arteries (139±42 to 167±73 μm, $p=0.19$, Table 1). The smallest visible artery was approximately 50 μm in diameter as judged from a reference copper wire with a diameter of 130 μm (double arrows).

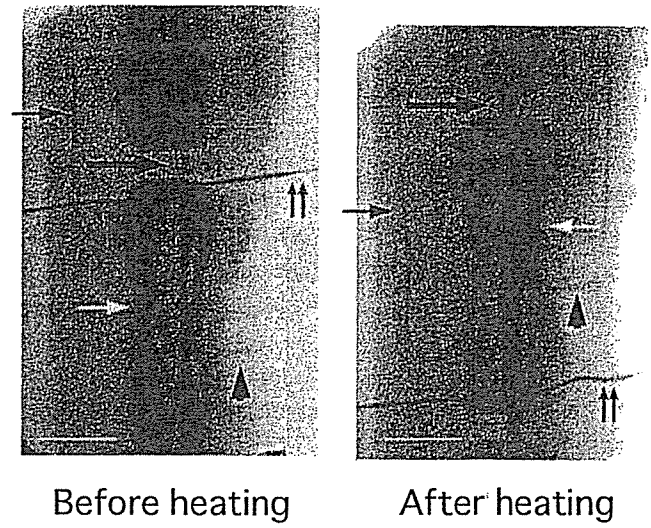

Fig. 2. Synchrotron radiation angiograms of rat tail before (left) and after heating (right). Large arrows, the medial caudal artery; small arrows, the lateral caudal arteries; arrowheads, segmental anastomosing vessels; white arrow, caudal vertebra; double arrows, reference copper wires with a diameter of 130 μm. Bar=3 mm.

The digital subtraction image processing allowed us to visualize the medial caudal artery, the lateral caudal arteries, and segmental anastomosing vessels more clearly even before heating (Fig. 3A). After heating, small string-like arteries with a diameter of approximately 60 μm were visualized beside the lateral caudal arteries and segmental anastomosing vessels (Fig. 3B–H, Table 1). These small arteries are considered to be the superficial caudal arteries based on the anatomical arrangement of rat tail arteries shown in a cross-

Table 1. Vasodilation to heat stress in rat tail arteries.

	Rectal temperature (°C) ($n=14$)	Diameter of the medial caudal artery (μm) ($n=14$)	Diameter of the lateral caudal artery (μm) ($n=14$)	Number of the superficial caudal arteries† ($n=5$)
Before heating	37.0±1.0	320±53	139±42	0±0
After heating	38.8±0.5	853±243*	167±73	7.4±2.4*

† Number of the superficial caudal arteries in one segment was counted. * $p<0.001$ vs. before heating (paired t-test).

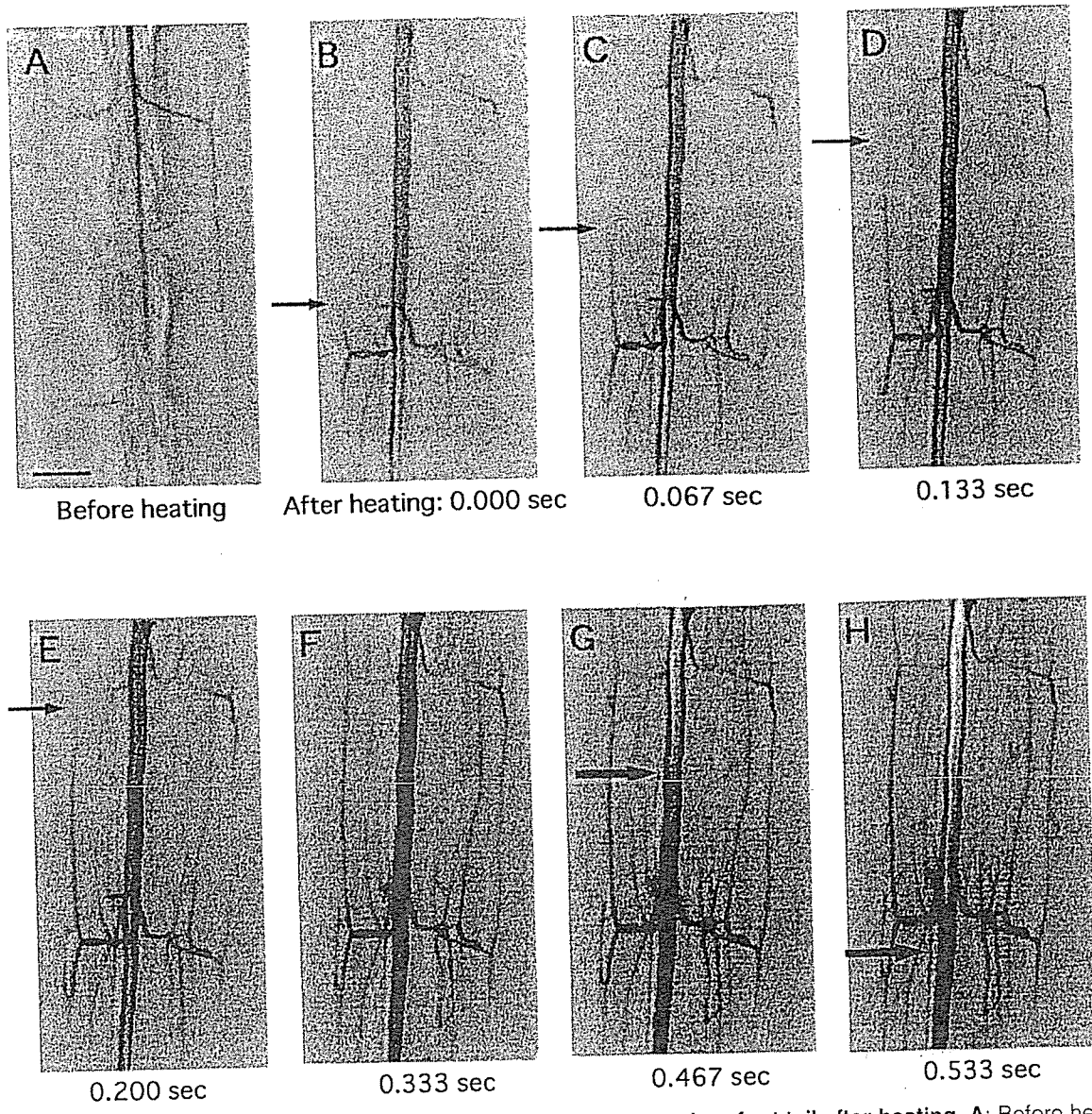

Fig. 3. Digitally subtracted images of synchrotron radiation angiography of rat tail after heating. A: Before heating. **B–H**: After heating. Elapsed time from panel B is shown in each panel. Small arrows, the top of the contrast material in the lateral caudal artery; large arrows, the top of the blood flow (the end of the contrast material) in the medial caudal artery. Bar=3 mm.

section of the tail (arrowheads in Fig. 4). Note that these arteries were not visualized before heating (Fig. 3A).

Sequential images after heating shown in Fig. 3B–H demonstrate that the direction of the blood flow in the medial caudal artery was from the base to the tip of the tail after heating (large arrows in Fig. 3). It was consistent with the direction of flow before heating (data not shown). On the other hand, in the lateral caudal artery, which was supplied by segmental anastomosing vessels arising from the medial caudal artery, the direction of the flow was not always from the base to the tip (small arrows in Fig. 3). Similar results were observed in the superficial caudal arteries, in which the flow was bidirectional (Fig. 3B–H). Arteriovenous anastomose-like stainings were not seen in these frames because venous images appear after the arterial images have faded completely (data not shown).

DISCUSSION

Since monochromatic synchrotron radiation enhances sensitivity for the iodine-contrast material and the high-definition video camera has high sensitivity and high resolution [10, 11], we were able to use these systems to perform microangiographies and visualize arteries as small as 50 μm in diameter in the rat tail, which has not been demonstrated *in vivo*.

Synchrotron radiation microangiography demon-

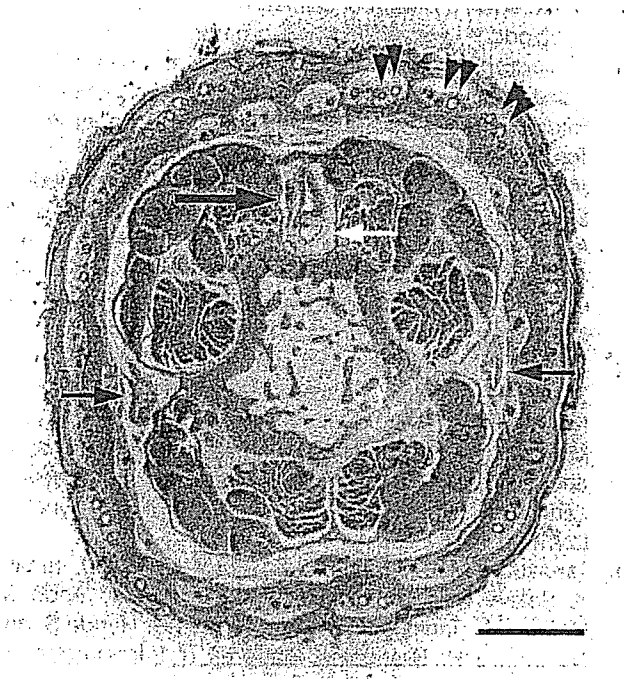

Fig. 4. Cross-section of the joint region of rat tail. The medial caudal artery (large arrow) and the lateral caudal arteries (small arrows) were present in the deep region of the tail. The superficial caudal arteries (arrowheads) were present in the superficial region. White arrow indicates the medial caudal vein. Hematoxylin and eosin stain. Original magnification ×1.25; Bar=2 mm.

strated that the rat tail possessed a dual set of arteries; It was shown that the medial caudal artery had high vasodilatory responsiveness to heat, but the vasodilatory response of the lateral caudal arteries and segmental anastomosing vessels was small. Furthermore, the superficial caudal arteries, which may remain closed or were very small before heating, showed marked vasodilatation after heating.

It is no surprise that arteries in the superficial region of the tail, such as the superficial caudal arteries, showed high sensitivity to the heat since their function is to perform heat-loss through the tail. The lateral caudal arteries did not respond to the heat, and therefore, their function presumably is not one of heat-loss but of feeding nutrients to the peripheral tissue. As such, they do not give significant flow to the superficial caudal arteries. Inhomogeneous dilation of tail vessels has been reported in rats in response to neuropeptide Y [7]. The administration of neuropeptide Y increased total tail blood flow but decreased superficial cutaneous flow in the tail. We previously reported that heat stress did not cause vasodilation in the skin (i.e., superficial inferior epigastric artery) in a rat evaluated by synchrotron radiation angiography [9]. Presumably, the abdominal subcutaneous vessel under the fur does not play an important role in thermoregulation in the rat. Similarly, the medial caudal artery is located in a relatively deep region in the tail and should not play a direct role in heat loss. The underlying mechanism for its marked dilation is a secondary effect of an increased flow to feed dilated superficial caudal arteries since the superficial caudal arteries are primarily fed by the medial caudal artery. Whether or not the medial caudal artery independently responds to heat is unclear.

Arteriovenous anastomoses are abundant in rat tail skin and play an important role in thermoregulation during heat stress [19]. Their diameters were shown to be relatively large since a large fraction of microspheres with a diameter of 15 μm injected to the medial caudal artery passed arteriovenous anastomoses [7]. However, we assume that the small arteries in Fig. 3 were not arteriovenous anastomoses but rather were superficial caudal arteries because all arteries were parallel and veins were stained at later stages. Unfortunately, the recording period of the present digital system was too short to demonstrate the venous phase.

Sequential images are advantageous for evaluating the direction of blood flow as shown in Fig. 3, and we were able to demonstrate bidirectional flow in the lateral caudal arteries and superficial caudal arteries.

The authors wish to thank Drs. Yoshiko Shinozaki, Takayuki Hasegawa, and Jobu Ito for their technical work. This work was supported by Grants-in-Aid for Scientific Research (12670064, 13470154, 13470381, 13877114, 14657460, 14657461) from the Ministry of Education, Culture, Sports, Science and Technology; The Science Frontier Program of MECSST; New Energy and Industrial Technology Development Organization; The Research Grants for Cardiovascular Disease (H13C-1) from the Ministry of Health, Labour and Welfare; and the Promotion Fundamental Studies in Health Science of the Organization for Pharmaceutical Safety and Research of Japan. This project was approved as a joint research program of the High Energy Accelerator Research Organization (98G181, 98G194, 98G195, 99G135, 01G182, and 02G160) and of Japan Synchrotron Radiation Research Institute.

REFERENCES

1. Armstrong CG and Kenney WL: Effects of age and acclimation on responses to passive heat exposure. J Appl Physiol 75: 2162–2167, 1993
2. Shido O and Nagasaka T: Heat loss responses in rats acclimated to heat loaded intermittently. J Appl Physiol 68: 66–70, 1990
3. Sakurada S, Shido O, Fujikake K, and Nagasaka T: Relationship between body core and peripheral temperatures at the onset of thermoregulatory responses in rats. Jpn J Physiol 43: 659–667, 1993

4. Rand RP, Burton AC, and Ing T: The tail of the rat, in temperature regulation and acclimatization. Can J Physiol Pharmacol 43: 257–267, 1965
5. Raman ER, Roberts MF, and Vanhuyse VJ: Body temperature control of rat tail blood flow. Am J Physiol 245: R426–R432, 1983
6. O'Leary DS and Johnson JM: Baroreflex control of the rat tail circulation in normothermia and hyperthermia. J Appl Physiol 66: 1234–1241, 1989
7. Heath ME: Neuropeptide Y and Y1-receptor agonists increase blood flow through arteriovenous anastomoses in rat tail. J Appl Physiol 85: 301–309, 1998
8. Young AA and Dawson NJ: Evidence for on-off control of heat dissipation from the tail of the rat. Can J Physiol Pharmacol 60: 392–398, 1981
9. Ito K, Tanaka E, Mori H, Nakazawa H, and Tanino R: A microangiographic technique using synchrotron radiation to visualize dermal circulation *in vivo*. Plast Reconstr Surg 102: 1128–1133, 1998
10. Tanaka E, Tanaka A, Sekka T, Shinozaki Y, Hyodo K, Umetani K, and Mori H: Digitized cerebral synchrotron radiation angiography: quantitative evaluation of the canine circle of Willis and its large and small branches. Am J Neuroradiol 20: 801–806, 1999
11. Mori H, Hyodo K, Tanaka E, Uddin MM, Yamakawa A, Shinozaki Y, Nakazawa H, Tanaka Y, Sekka T, Iwata Y, Handa S, Umetani K, Ueki H, Yokoyama T, Tanioka K, Kubota M, Hosaka H, Ishikawa N, and Ando M: Small-vessel radiography *in situ* with monochromatic synchrotron radiation. Radiology 201: 173–177, 1996
12. Takeshita S, Isshiki T, Mori H, Tanaka E, Eto K, Miyazawa Y, Tanaka A, Shinozaki Y, Hyodo K, Ando M, Kubota M, Tanioka K, Umetani K, Ochiai M, Sato T, and Miyashita H: Use of synchrotron radiation microangiography to assess development of small collateral arteries in a rat model of hindlimb ischemia. Circulation 95: 805–808, 1997
13. Tanaka Y, Mori H, Tanaka E, Abe S, Makuuchi H, Nakazawa H, Handa S, Tanioka K, Kubota M, Kumaoka S, Hyodo K, and Ando M: Synchrotron radiation microangiography using an avalanche-type high-definition video camera. *In*: Medical Applications of Synchrotron Radiation, ed. Ando M and Uyama C, Springer-Verlag, Tokyo, pp 42–53, 1998
14. Mori H, Tanaka E, Hyodo K, Uddin Mohammed M, Sekka T, Ito K, Shinozaki Y, Tanaka A, Nakazawa H, Abe S, Handa S, Kubota M, Tanioka K, Umetani K, and Ando M: Synchrotron microangiography reveals configurational changes and to-and-fro flow in intramyocardial vessels. Am J Physiol 276: H429–H437, 1999
15. Sekka T, Volchikhina SA, Tanaka A, Hasegawa M, Tanaka Y, Ohtani Y, Tajima T, Makuuchi H, Tanaka E, Iwata Y, Sato S, Hyodo K, Ando M, Umetani K, Kubota M, Tanioka K, and Mori H: Visualization, quantification, and therapeutic evaluation of angiogenic vessels in cancer by synchrotron microangiography. J Synchrotron Rad 7: 361–367, 2000
16. Tanaka A, Mori H, Tanaka E, Mohammed MU, Tanaka Y, Sekka T, Ito K, Shinozaki Y, Hyodo K, Ando M, Umetani K, Tanioka K, Kubota M, Abe S, Handa S, and Nakazawa H: Branching patterns of intramural coronary vessels determined by microangiography using synchrotron radiation. Am J Physiol 276: H2262–H2267, 1999
17. Tanioka K, Yamazaki J, Shidara K, Taketoshi K, Kawamura T, Hirai T, and Takasaki Y: Avalanche-mode amorphous selenium photoconductive target for camera tube. Adv Electronics Electron Phys 74: 379–387, 1988
18. Umetani K, Ueki H, Takeda T, Itai Y, Mori H, Tanaka E, Mohammed MU, Shinozaki Y, Akisada M, and Sasaki Y: High-spatial-resolution and real-time medical imaging using a high-sensitivity HARPICON camera. J Synchrotron Rad 5: 1130–1132, 1998
19. Gemmell RT and Hales JR: Cutaneous arteriovenous anastomoses present in the tail but absent from the ear of the rat. J Anat 124: 355–358, 1977

Molecular Biology of the Cell
Vol. 13, 4231–4242, December 2002

Adaptor Protein Crk Is Required for Ephrin-B1-induced Membrane Ruffling and Focal Complex Assembly of Human Aortic Endothelial Cells[V]

Ken-Ichiro Nagashima,* Akira Endo,* Hisakazu Ogita,* Akiko Kawana,* Akiko Yamagishi,* Akira Kitabatake,† Michiyuki Matsuda,‡ and Naoki Mochizuki*§

*Department of Structural Analysis, National Cardiovascular Center Research Institute, Suita, Osaka 565-8565, Japan; †Department of Cardiovascular Medicine, Hokkaido University School of Medicine, Sapporo 060-6833, Japan; and ‡Department of Tumor Virology, Research Institute for Microbial Diseases, Osaka University, Osaka 565-0871, Japan

Submitted April 4, 2002; Revised July 18, 2002; Accepted August 29, 2002
Monitoring Editor: Richard K. Assoian

Endothelial cell migration is an essential step in vasculogenesis and angiogenesis, in which receptor tyrosine kinases play a pivotal role. We investigated the mechanism by which ephrin-B1 promotes membrane ruffling in human aortic endothelial cells, because membrane ruffling heralds cell body migration. We especially focused on the role of Crk adaptor protein in EphB-mediated signaling. Using DsRed-tagged Crk and a fluorescent time-lapse microscope, we showed that Crk was recruited to the nascent focal complex after ephrin-B1 stimulation. Furthermore, we found that $p130^{Cas}$, but not paxillin, recruited Crk to the nascent focal complex. The necessity of Crk in ephrin-B1–induced membrane ruffling was shown both by the overexpression of dominant negative Crk mutants and by the depletion of Crk by using RNA interference. Then, we examined the role of two major downstream molecules of Crk, Rac1 and Rap1. The dominant negative mutant of Rac1 completely inhibited ephrin-B1–induced membrane ruffling and focal complex assembly. In contrast, rap1GAPII, a negative regulator of Rap1, did not inhibit ephrin-B1–induced membrane ruffling. However, in rap1GAPII-expressing cells, ephrin-B1 did not induce membrane spreading, probably due to instability of the focal complex. These results indicated that Crk plays a critical role in Rac1-induced membrane ruffling and Rap1-mediated nascent focal complex stabilization contributing to ephrin-B1–induced human aortic endothelial cells migration.

INTRODUCTION

Vasculogenesis and angiogenesis are the two major processes of vascular formation in physiological and pathological conditions, including embryogenesis, ovulation, wound healing, tumorigenesis, and ischemic diseases (Yancopoulos *et al.*, 1998; Carmeliet and Jain, 2000). Vascular endothelial cells are involved in both processes. Endothelial precursor cells proliferate and differentiate to mature endothelial cells to form the primary capillary in vasculogenesis, whereas sprouting of endothelial cells is the initial step of angiogenesis (Risau, 1997). Migration of the vascular endothelial cell is regulated by the combinations of tyrosine kinase receptors and their cognate ligands such as vascular endothelial growth factor receptor/vascular endothelial growth factor, Tie receptor/Angiopoietin, and Eph/ephrin (Yancopoulos *et al.*, 1998, 2000).

Eph receptors consist of two subgroups: EphA receptors bind to glycosylphosphatidylinositol-anchored proteins, ephrin-A, whereas EphB receptors bind to transmembrane proteins, ephrin-B (Eph Nomenclature Committee, 1997). Knowledge of the distribution of the members of Eph/ephrin is still limited. Although arterial endothelial cells

Article published online ahead of print. Mol. Biol. Cell 10.1091/mbc.E02–04–0181. Article and publication date are at www.molbiolcell.org/cgi/doi/10.1091/mbc.E02–04–0181.

[V] Online version of this article contains video material for some figures. Online version available at www.molbiolcell.org.

§ Corresponding author. E-mail address: nmochizu@ri.ncvc.go.jp.

Abbreviations used: CFP, cyan fluorescent protein; ECM, extracellular matrix; EGFP, enhanced green fluorescent protein; FBS, fetal bovine serum; FRET, fluorescent resonance energy transfer; GAP, GTPase-activating protein; GEF, guanine nucleotide exchange factor; HAEC, human aortic endothelial cell; IRES, internal ribosomal entry site; SH, Src homology; siRNA, small interfering RNA; YFP, yellow fluorescent protein.

have been marked by ephrin-B2, venous endothelial cells have been marked by EphB4 (Wang *et al.*, 1998; Gale *et al.*, 2001). However, Shin *et al.* (2001) have recently reported that EphB4 is expressed in the aorta and other arteries.

EphB receptor and ephrin-B ligand work reciprocally. Their engagement activates downstream signaling of both EphB and ephrin-B (Brückner *et al.*, 1997; Dodelet and Pasquale, 2000). Recently, two ephrin-B1–binding proteins, PDZ-RGS3 (Lu *et al.*, 2001) and Grb4 (Cowan and Henkemeyer, 2001), have been shown to regulate cell migration. EphB receptors, on the other hand, provide autophosphorylated tyrosine residues as docking sites for the Src homology (SH)2-containing molecules such as p120-RasGAP, Fyn (Hock *et al.*, 1998), Abl (Yu *et al.*, 2001), Grb2, Grb10 (Stein *et al.*, 1996), Src, Crk (Zisch *et al.*, 2000), and SHEP1 (Dodelet *et al.*, 1999). However, involvement of these SH2-containing molecules in EphB-dependent cellular migration has not been demonstrated to date.

Crk is an adaptor protein that links phosphotyrosine-containing molecules and SH3-binding molecules (Kiyokawa *et al.*, 1997). Alternative splicing of the human *crk* gene generates two Crk proteins: CrkII consists of an SH2 and two SH3 domains, whereas CrkI lacks the carboxy-terminal SH3 of CrkII (Matsuda *et al.*, 1992) (Figure 1A). The SH2 domain of Crk binds several phosphotyrosine-containing proteins, including $p130^{Cas}$ (Sakai *et al.*, 1994) and paxillin (Birge *et al.*, 1993; Schaller and Parsons, 1995), whereas the SH3 domain of CrkII and CrkI binds to proteins, including C3G and DOCK180 (reviewed in Kiyokawa *et al.*, 1997). C3G and DOCK180 have been shown to activate the low-molecular-weight G proteins Rap1 and Rac1, respectively; therefore, Crk functions as an adaptor protein connecting tyrosine kinases to G proteins.

Involvement of Crk in cellular migration has been extensively studied using *Caenorhabditis elegans*, *Drosophila melanogaster*, and mammalian cells. We have shown that a Crk SH3-binding protein, DOCK180, induces membrane ruffling via Rac1 (Kiyokawa *et al.*, 1998). In *D. melanogaster*, nonfunctional mutation in *myoblast city*, a homolog of DOCK180, results in the failure of dorsal closure due to abnormal cell migration (Erickson *et al.*, 1997). *Ced*-2, *Ced*-5, and *Ced*-10 of *C. elegans* have been isolated as genes essential for the phagocytosis of apoptotic bodies and subsequently identified as homologues of mammalian *crk*, *DOCK180*, and *rac*, respectively (Wu and Horvitz, 1998; Reddien and Horvitz, 2000). Therefore, the Crk-DOCK180-Rac1 pathway is conserved from nematodes to humans and plays a critical role in cell migration and phagocytosis.

Another SH3-binding partner, C3G, has been shown to participate in cell adhesion to extracellular matrix (ECM) via Rap1 activation (Ohba *et al.*, 2001; Li *et al.*, 2002). We have demonstrated that C3G-deficient mouse embryonic fibroblasts show impaired cell adhesion and delayed cell spreading (Ohba *et al.*, 2001). Li *et al.* (2002) have shown that Src, Crk, C3G, and Rap1 regulate the stability of focal adhesions.

Cell migration requires membrane extension, assembly of cell contacts to ECM in the leading edge, destabilization of those in the rear of the cell, and increased locomotive forces (Lauffenburger and Horwitz, 1996). Membrane extension, which includes filopodia and lamellipodia, is regulated by Rho-family GTPases (Bar-Sagi and Hall, 2000). Cell contacts to ECM are largely classified into three subgroups by their morphology. Focal complexes are dot-like structures at the leading edge of the lamellipodia. Focal adhesions are adhesions larger than focal complexes mostly found in the peripheral region of cells. Fibrillar adhesions are elongated structures located predominantly in the central region of

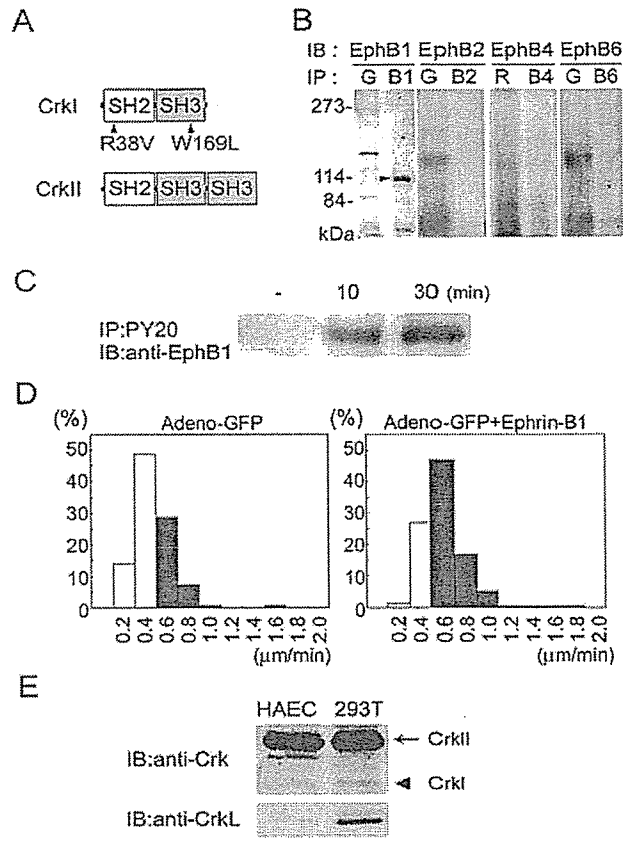

Figure 1. HAECs express EphB1 and respond to ephrin-B1. (A) Schematic illustration of CrkI, CrkII, and mutants. Arrowheads indicate the mutation in CrkI-R38V (Arg at 38 replaced with Val) and CrkI-W169L (Trp at 169 replaced with Leu). (B) HAEC lysates were incubated with antibodies as indicated (IP), followed by SDS-PAGE, and immunoblotting with antibodies as indicated (IB). The position of EphB1 is indicated by the arrowhead. For the immunoprecipitation, species-matched normal serum, goat (G), or rabbit (R) was used. B1, anti-EphB1; B2, anti-EphB2; B4, anti-EphB4; and B6, anti-EphB6. (C) Lysates of HAECs stimulated with preclustered ephrin-B1/Fc for time as indicated at the top were immunoprecipitated with anti-phosphotyrosine antibody (PY20). Precipitates were subjected to SDS-PAGE and immuboblotted with anti-EphB1. (D) Ephrin-B1–induced HAECs migration was examined for the migratory velocity of GFP-expressing HAECs. HAECs (150) infected with a recombinant adenovirus expressing GFP were left unstimulated (left) or were stimulated (right) with preclustered 1 μg/ml soluble ephrin-B1/Fc. Cells were tracked by MetaMorph 4.6 software and analyzed for their mean migratory velocity. The details of the analysis are described in MATERIALS AND METHODS. Cells moving >0.6 μm/min are shown in the black column. (E) Cell lysates of 293T cells and HAECs were subjected to SDS-PAGE and immunoblotted with antibodies as indicated at the left. Arrow and arrowhead indicated CrkII and CrkI, respectively.

cells (Rottner *et al.*, 1999; Geiger *et al.*, 2001). The latter two structures are connected to actin stress fibers.

In this study, we investigated the role of Crk in ephrin-B1–induced endothelial cell migration. We demonstrate that the ephrin-B1–induced membrane ruffling is mediated by the Crk-Rac1 pathway and that the assembly and maturation of focal complexes is regulated by the Crk-Rap1 pathway.

MATERIALS AND METHODS

Reagents and Antibodies

Recombinant soluble mouse ephrin-B1-human Fc chimeric protein (ephrin-B1/Fc) (Stein *et al.*, 1996) was purchased from R & D Systems (Minneapolis, MN). Ephrin-B1/Fc was preclusterd by goat anti-human Fc before the stimulation and used at 1 μg/ml throughout this study. Protein A- and G-Sepharose were from Calbiochem (La Jolla, CA). Type-I collagen used for coating glass-base dishes was purchased from Nitta Gelatin (Osaka, Japan). Anti-EphB1, anti-EphB2, anti-EphB4, anti-EphB6, and anti-CrkL were from Santa Cruz Biotechnology (Santa Cruz, CA); anti-human Fc was from R & D Systems; antipaxillin was from Zymed Laboratories (South San Francisco, CA); anti-β-tubulin and anti-actin were from Sigma-Aldrich (St. Louis, MO); and anti-phosphotyrosine (PY20), anti-Crk, and anti-p130^{Cas} were from Transduction Laboratories (Lexington, KY).

Plasmids

pCA-DsRed-CrkI was derived from pCAGGS eukaryotic expression vector and expressed DsRed-tagged CrkI (Niwa *et al.*, 1991). pIRM21 and pCXN2-FLAG-IRES (internal ribosomal entry site)-enhanced green fluorescent protein (EGFP) (Ichiba *et al.*, 1999) were expression vectors derived from pCAGGS and contained internal ribosome entry site (IRES) and the coding region of dsFP593 and EGFP, respectively, at the 3′ side of the multiple cloning site. Synthesized cDNA encoding dsFP593 (Fradkov *et al.*, 2000) was obtained from A. Miyawaki (RIKEN, Wako-shi, Japan). The DNA fragments encoding CrkI substituted at Arg^{38} for Val in the SH2 domain, or CrkI substituted at Trp^{169} for Leu in the SH3 domain, hereafter R38V or W169L, respectively, were amplified by polymerase chain reaction and subcloned into pIRM21 or pCXN2-FLAG-IRES-EGFP, respectively. pCXN2-FLAG-Rac1N17-IRES-EGFP expressed both FLAG-tagged Rac1 at Ser^{17} substituted for Asn and EGFP. pCXN2-FLAG-rap1GAPII-IRES-EGFP expressed both FLAG-tagged rap1GAPII and EGFP. pEGFP-actin was purchased from CLONTECH (Palo Alto, CA). All of the DNA fragments amplified by polymerase chain reaction were ligated into pCR-BluntII-TOPO vector (Invitrogen, Carlsbad, CA), and the sequence was confirmed with an ABI Prism 3700 (Applied Biosystems Japan, Tokyo, Japan).

Virus

We have previously developed the in vivo Ras or Rap1 activation monitoring probes Raichu-Ras or Raichu-Rap1, respectively. Briefly, Raichu-Ras consists of yellow fluorescent protein (YFP), H-Ras, Ras-binding domain of Raf, cyan fluorescent protein (CFP), and the CAAX box of Ki-Ras, whereas Ras is replaced by Rap1 in Raichu-Rap1 (Mochizuki *et al.*, 2001) (Figure 7A). We produced recombinant adenoviruses, Adeno-Raichu-Ras, and -Rap1 by Adeno-X system according to the manufacturer's protocol (CLONTECH). DNA encoding Raichu-Ras was ligated into pShuttle vector. An expression cassette was cleaved out from pShuttle-derived vector and ligated into pAdeno-X. The adenovirus genome was cut out from pAdeno-X-derived vector and transfected into human embryonic kidney (HEK)293 cells. A recombinant adenovirus expressing Raichu-Ras was produced during 2 wk. Adenovirus expressing Raichu-Rap1 was produced in a similar manner to Raichu-Ras. A recombinant adenovirus for green fluorescent protein (GFP) expression was obtained from H. Kurose (Kyushu University, Kyushu, Japan). Adenovirus expressing CrkI-W169L and EGFP, Adeno-CrkI-W169L, was produced as reported previously (Endo *et al.*, 2002). Briefly, DNA encoding CrkI-W169L, IRES, and EGFP from pCXN2-FLAG-CrkI-W169L-IRES-EGFP was ligated into pShuttle. A recombinant virus was produced in a similar manner to Adeno-Raichu-Ras. pIRM21-CrkI-R38V was used to produce Adeno-CrkI-R38V expressing CrkI-R38V and dsFP593.

Cells, Transfection, and Infection

Human aortic endothelial cells (HAECs) were purchased from Cascade Biologics (Portland, OR). HEK293 cells were from American Type Culture Collection (Manassas, VA). 293T cells were provided by B.J. Mayer (University of Connecticut, Storrs, CT). HAECs were maintained in HuMedia-EG2 (Kurabo, Kurashiki, Japan) supplemented with a growth additive set containing 2% fetal bovine serum (FBS), 10 ng/ml human epidermal growth factor, 1 μg/ml hydrocortisone, 50 μg/ml gentamicin, 50 ng/ml amphotericin B, 5 ng/ml human fibroblast growth factor, and 10 μg/ml heparin. HAECs were used before passage 7. HEK293 cells and 293T cells were cultured in DMEM (Invitrogen) supplemented with 10% FBS, 2 mM L-glutamine. HEK293 cells were transfected by calcium phosphate. HAECs cultured on a collagen-coated 35-mm-diameter glass-base dish (Asahi Techno Glass, Tokyo, Japan) were transfected with 3 μg of plasmid DNA by using LipofectAMINE PLUS reagent (Invitrogen) or infected with adenovirus at the appropriate multiplicity of infection for the time periods as indicated in the figure legends. HAECs were starved for >8 h before the stimulation in DMEM/F-12 (Invitrogen) without phenol red supplemented with 2 mM L-glutamine, 10 mM HEPES, 1.2 g/l $NaHCO_3$, and 0.5% bovine serum albumin fraction V.

RNA interference

Small interfering RNAs (siRNA) corresponding to the bases 264–284 of human CrkII coding sequence 5′-AAUAGGAGAUCAAGAGUUUGA-3′ and 5′-UCAAACUCUUGTUCUCCUTUU-3′ (Dharmacon Research, Lafayette, CO) were annealed and transfected into 293T cells or HAECs by using OligofectAMINE (Invitrogen).

Immunoprecipitation, Immunoblotting, and Cell Staining

HAECs were washed with Tris-buffered saline containing 1 mM Na_3VO_4 and lysed in lysis buffer (150 mM NaCl, 20 mM Tris hydrocloride, pH 7.5, 1.5 mM $MgCl_2$, 1 mM Na_3VO_4, 1% Triton X-100, 10 mM NaF, and protease inhibitor cocktail; Roche Applied Science, Basel, Switzerland). Lysates were precleard by centrifugation at 15,000 × *g* for 10 min, followed by immunoprecipitation by using antibodies indicated in the figure and protein A- or G-Sepharose (Calbiochem). Immunoprecipitates were subjected to SDS-PAGE and immunoblotting with antibodies as indicated in the figure. Proteins reacting with primary antibodies were visualized by an enhanced chemiluminescence system (Amersham Biosciences UK, Little Chalfont, Buckinghamshire, United Kingdom) for detecting peroxidase-conjugated secondary antibodies and analyzed with an LAS-1000 system (Fuji Film, Tokyo, Japan). Quantitative analyses of immunoblots were performed using Image Gauge version 3.4X software included in LAS-1000 system. HAECs transfected with pCA-DsRed-CrkI cultured on a collagen-coated glass-base dish were stimulated with preclustered ephrin-B1/Fc for 20 min. Cells washed with phosphate-buffered saline were fixed by 4% paraformaldehyde at room temperature, followed by permeabilization with 0.1% Triton X-100. Permeabilized cells were incubated with anti-p130^{Cas} or anti-paxillin antibody. Proteins reacting with anti-

bodies were detected with Alexa 488 goat anti-mouse IgG (Molecular Probes, Eugene, OR). Confocal images for DsRed-CrkI, $p130^{Cas}$, and paxillin were obtained by a BX50WI microscope controlled by Fluoview (Olympus, Tokyo, Japan).

Time-Lapse Imaging

HAECs transfected with plasmids expressing fluorescence-tagged proteins or IRES-driven fluorescence or infected with adenovirus expressing IRES-driven fluorescence were imaged on an IX-70 inverted microscope (Olympus). The microscope with a 75-W xenon arc lamp was equipped with a cooled charge-coupled device camera, CoolSNAP-HQ (Roper Scientific, Trenton, NJ), and two filter changers, controlled by MetaMorph 4.6 software (Roper Scientific). Both the EGFP image and the DsRed/dsFP593 image were obtained through an XF2043 dichroic filter (Omega Optical, Brattleboro, VT) and a set of an S484/15 excitation filter and an S515/30 emission filter (Chroma Technology, Brattleboro, VT) for EGFP and a set of an S555/25 excitation filter and an S630/60 emission filter for DsRed and dsFP593. To monitor cell shape and localization of fluorescence-tagged proteins, a phase-contrast image and a fluorescence image were obtained every 20 s. A series of time-lapse images were converted to video format by using MetaMorph 4.6 software.

Cell Motility Analysis and Quantitative Analysis of Membrane Ruffling

The motility of HAECs was analyzed as described previously (Ohba *et al.*, 2001). Briefly, HAECs infected with recombinant GFP expressing adenovirus were spread on a collagen-coated glass-base dish and cultured in DMEM supplemented with 1% FBS for 8 h before exposure to preclustered ephrin-B1/Fc. GFP-expressing HAECs were tracked for 6 h after the stimulation by using a fluorescent microscopy in a series of time-lapse images collected using MetaMorph 4.6 software. The distance between the point where HAECs attached and the end point where HAECs moved was measured by tracing cells. The mean velocity was obtained by the distance divided by the period during which cells were tracked. The migration velocity of HAECs was analyzed by a cell-tracking system included in MetaMorph 4.6. For quantitative analysis of membrane ruffling, uninfected HAECs and those infected with either Adeno-CrkI-R38V or Adeno-CrkI-W169L were cocultured on the same dish, starved for 8 h, and exposed to preclustered ephrin-B1/Fc. A phase-contrast image and a fluorescence image were recorded first, and a sequential phase-contrast image was obtained every 20 s. A series of time-lapse images were converted to a video by MetaMorph 4.6. Ephrin-B1–induced membrane extension reflecting the membrane ruffling was quantified by measuring the cell size before and after ephrin-B1/Fc stimulation. The cell size was analyzed by a region measurement tool included in MetaMorph 4.6. HAECs transfected with either pCXN2-FLAG-Rac1N17-IRES-EGFP or pCXN2-FLAG-rap1GAPII-IRES-EGFP were analyzed for ephrin-B1–induced membrane extension similarly to those infected with Adeno-CrkI mutants.

Fluorescent Resonance Energy Transfer (FRET) Imaging

HAECs cultured on a collagen-coated 35-mm-diameter glass-base dish were infected with adenovirus as indicated in the figure legends and stimulated with preclustered ephrin-B1/Fc. Cells were imaged on an IX-70 inverted microscope (Olympus) in a method similar to time-lapse imaging. CFP and YFP images were obtained through a filter set with a XF1071 excitation filter, a XF2034 dichroic mirror, and a XF3075 emission filter for CFP and a XF3079 for YFP (Omega Optical), respectively. The emission ratio of YFP/CFP and the intensity of CFP were used for imaging of FRET in the intensity modulated display mode controlled by MetaMorph 4.6. A series of time-lapse images obtained every 20 s were converted to a video by using MetaMorph 4.6.

RESULTS

Ephrin-B1 Accelerates the Motility of HAECs

We first examined the expression of EphB-family receptors in HAECs by using antibodies against EphB1, EphB2, EphB4, and EphB6 (Figure 1B). Among them, only EphB1 was detected in HAECs (Figure 1B). To test whether EphB1 was indeed activated upon ephrin-B1, a ligand for EphB1, HAECs were stimulated with preclustered ephrin-B1/Fc. Ephrin-B1-dependent phosphorylation of EphB1 was observed for 30 min (Figure 1C). We then proceeded to test the effect of ephrin-B1 on the motility of HAECs. For the migration assay, HAECs were marked with GFP-carrying adenovirus and stimulated with preclustered ephrin-B1/Fc. Cells were tracked under a fluorescent time-lapse microscope, and the velocity of each cell was calculated. Approximately 35% of unstimulated HAECs moved >0.6 mm/min as shown in the black column (Figure 1D, left), whereas ~70% of those stimulated with ephrin-B1 did similarly (Figure 1D, right), demonstrating that ephrin-B1 significantly accelerated cell migration. HAECs stimulated with preclustered Fc did not show any acceleration in the cell migration (our unpublished data). In the following experiments, the involvement of Crk in the ephrinB1-induced signaling was examined. Therefore, we examined the expression of CrkII and CrkI, which are alternatively spliced products of *Crk* gene, and that of CrkL, a Crk-related protein consisting of a SH2 and two SH3 domains similar to CrkII. CrkII was predominantly expressed in 293T cells and HAECs, although CrkI was detected in both cells, whereas CrkL was detected in 293T cells, but not in HAECs (Figure 1E).

Crk Is Translocated to the Nascent Focal Complexes upon Ephrin-B1 Stimulation in HAECs

In ephrin-B1–stimulated cells, prominent membrane ruffling always preceded the cell body migration. Therefore, in the following experiments, we focused on the role of Crk, which is known to regulate cell migration in fibroblasts, in the ephrin-B1–induced membrane ruffling. Localization of Crk was monitored by the expression of DsRed-tagged CrkI with a time-lapse fluorescent microscope (Figure 2A, top). By monitoring the coexpression of EGFP-actin, we simultaneously observed the organization of actin stress fiber. Before ephrin-B1 stimulation, Crk was localized at focal or fibrillar adhesions both in the center and periphery of the cells. In the overlay images of Crk and actin, actin stress fibers were shown to bridge the accumulated Crk in the center and the periphery of the cells, indicating that Crk was localized to focal and fibrillar adhesions (Figure 2A, bottom, and Video 2A2). On ephrin-B1 stimulation, Crk was translocated to the leading edge of spreading membrane ruffles. The accumulation of Crk in membrane ruffles formed dots smaller than those found in the center of quiescent cells (Figure 2A, top, and Video 2A1). These nascent accumulations of Crk were not yet connected to actin stress fiber, indicating that these were focal complexes (Figure 2B). Next, we observed the course of the nascent focal complexes in consecutive images. Some focal complexes became larger

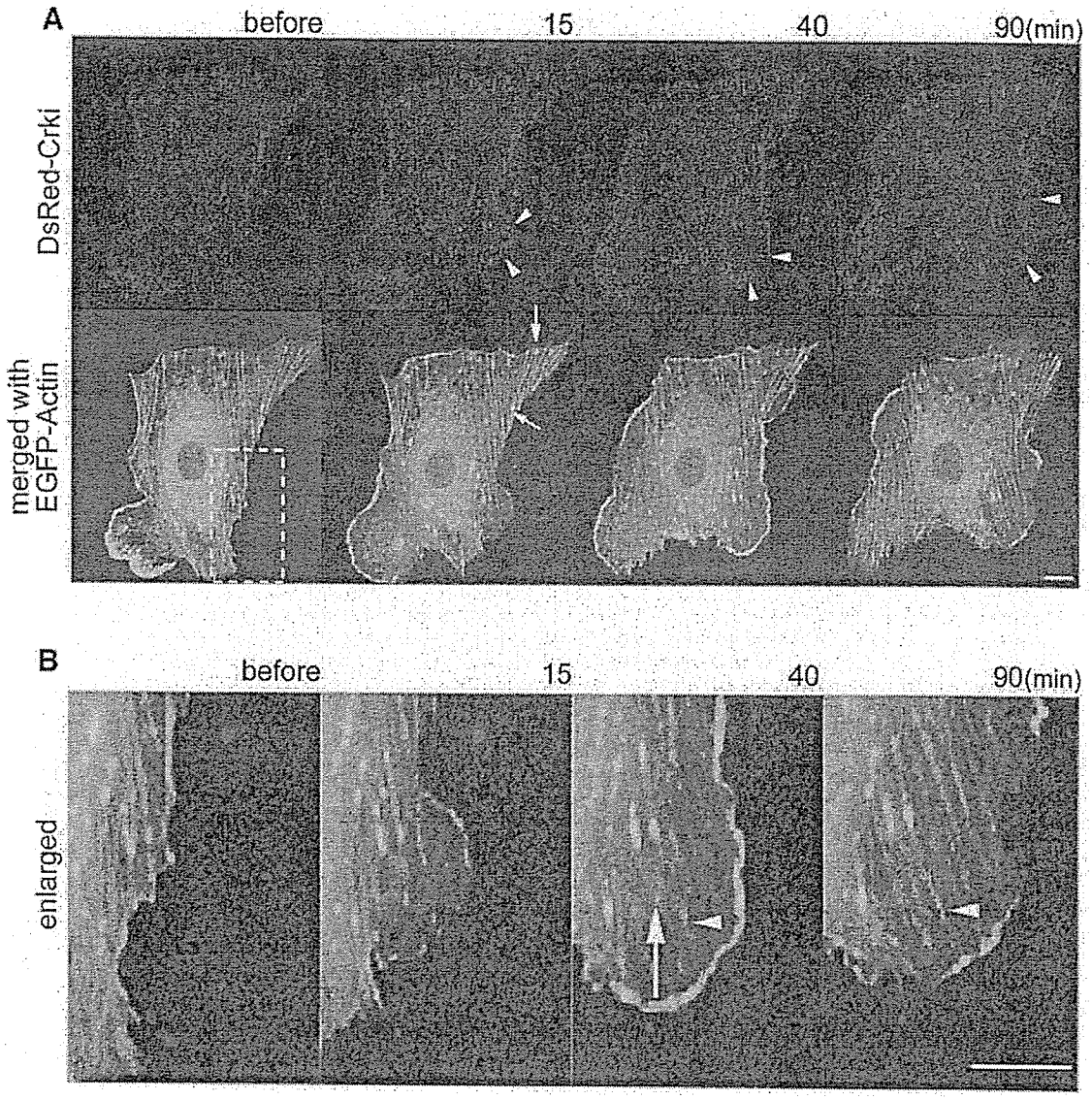

Figure 2. CrkI is translocated to nascent focal complexes upon ephrin-B1 stimulation and is involved in the development of focal adhesion. HAECs cultured on a collagen-coated glass-base dish were transfected with pCA-DsRed-CrkI, starved for 8 h, and stimulated with preclustered 1 μg/ml soluble ephrin-B1/Fc. EGFP-actin and DsRed-CrkI were imaged on an IX-70 inverted microscope (Olympus). A series of DsRed and EGFP images were collected by MetaMorph 4.6 software. Before, before the stimulation; 15, 40, and 90 min, time for stimulation. Bar, 10 μm. (A) Arrowheads indicate typical accumulation of DsRed-CrkI to nascent focal complexes (top). The GFP image of the same cell transfected with pEGFP-actin was merged with the DsRed-CrkI image (bottom). Arrows indicate an example of focal adhesions connecting actin stress fiber (also see Video 2A2). (B) The boxed region in the lower panel of A was enlarged. An arrow indicates a focal complex detached from the substratum and floating in membrane ruffles. The arrowhead indicates the development of a focal complex to a focal adhesion (also see Video 2B).

and connected with actin stress fiber, showing the development of focal complexes to focal adhesions (Figure 2B, white arrowhead, and Video 2B). On the other hand, some focal complexes detached from the substratum (Figure 2B, white arrow, and Video 2B) and disappeared or moved toward the center of the cell. These results indicated that Crk was involved in the assembly and maturation of the focal complexes in ephrin-B1–stimulated HAECs.

Crk Preferentially Colocalizes with p130^{Cas} at the Focal Complexes in HAECs upon Ephrin-B1 Stimulation

The two major SH2-binding partners of Crk in cell adhesion have been identified as p130^{Cas} and paxillin (Schaller and Parsons, 1995; Vuori *et al.*, 1996). To understand the role of Crk at the focal complexes, we examined the colocalization

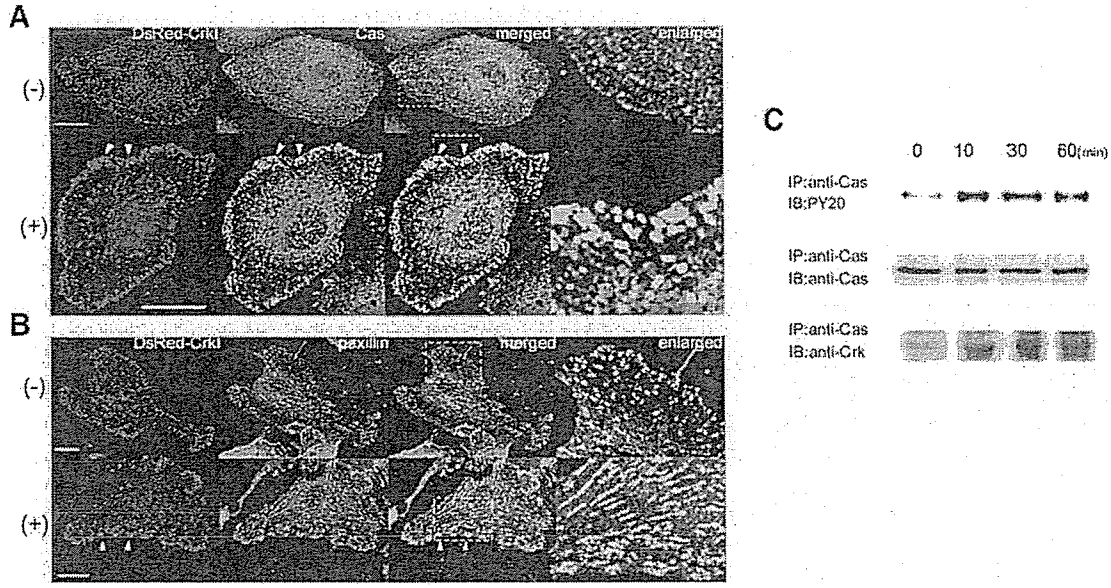

Figure 3. CrkI colocalizes with p130^{Cas} at the focal complexes upon ephrin-B1 stimulation. (A) HAECs expressing DsRed-CrkI plated on the glass-base dish were starved for 8 h and stimulated with 1 μg/ml preclustered ephrin-B1/Fc for 20 min. Cells were fixed with 4% paraformaldehyde, permeabilized with 0.1% Triton X-100, and incubated with antip130^{Cas} antibody. Immunoreactive protein was visualized by Alexa 488 goat anti-mouse IgG. Confocal images for DsRed-CrkI and p130^{Cas} were obtained by a BX50WI microscope controlled by Fluoview (Olympus). An image for p130^{Cas} (green) and an image for DsRed-CrkI (red) were superimposed (merged). Arrowheads indicate focal complexes. The boxed region was enlarged and is shown in the right panel (enlarged). Note that DsRed-CrkI colocalizes with p130^{Cas} at the focal complex after the stimulation, as indicated by the yellow spots. (B) Similar experiments were performed with anti-paxillin antibody. Arrowheads indicate focal complexes. The boxed region was enlarged. Note that DsRed-CrkI (red) and paxillin (green) colocalizes mostly at the fibrillar adhesions and focal adhesions of the center of the cell. −, before ephrin-B1 stimulation; +, 20 min after the stimulation; Bar, 20 μm. (C) Lysates of HAECs stimulated with preclustered ephrin-B1/Fc for time period as indicated at the top were immunoprecipitated as indicated at the left. Immunoprecipitates were subjected to SDS-PAGE and immunoblotted with antibodies as indicated at the left.

of Crk and the two SH2-binding proteins of Crk, p130^{Cas} and paxillin (Figure 3). In unstimulated HAECs, p130^{Cas} was condensed at the perinuclear region. Colocalization of Crk with p130^{Cas} was not obvious. After ephrin-B1 stimulation, p130^{Cas} was accumulated at the focal complexes, where DsRed-CrkI was also translocated (Figure 3A). We next examined the localization of paxillin (Figure 3B). In unstimulated cells, paxillin was localized at the focal adhesions and fibrillar adhesions. Colocalization of Crk with paxillin was observed throughout the cell, but its presence was more profound at the peripheral focal adhesion. The ephrin-B1 stimulation induced the accumulation of Crk at the focal complex and peripheral focal adhesion; however, paxillin was not recruited to these nascent focal adhesions. These results suggested that the accumulation of phosphorylated p130^{Cas} recruited Crk to the focal complex in ephrin-B1–stimulated HAECs. We further confirmed that ephrinB1-induced p130^{Cas} phosphorylation, which is indispensable for its association with Crk (Kiyokawa *et al.*, 1997). HAECs were stimulated with preclustered ephrin-B1/Fc for time period indicated at the top (Figure 3C). p130^{Cas} was phosphorylated (Figure 3C, top) and associated with endogeneous Crk (Figure 3C, bottom) upon ephrin-B1 stimulation.

Crk Is Responsible for Ephrin-B1–induced Membrane Ruffling in HAECs

To assess the physiological role of Crk in the ephrin-B1–induced membrane ruffling, we used the adenovirus-mediated overexpression of dominant negative mutants of Crk (Figure 1A). CrkI-R38V consists of a nonfunctioning SH2 and an intact SH3, thus serving to sequester SH3-binding proteins. Similarly, CrkI-W169L, which consists of an intact SH2 and a nonfunctioning SH3, blocks the phosphotyrosine residues. We have previously shown that CrkI-W169L and CrkI-R38V work as dominant negative mutants for CrkI/II (Ichiba *et al.*, 1997, 1999). The expression of dominant negative CrkI in HAECs infected with adenovirus carrying CrkI mutant for 24 h was comparable to the endogeneous CrkII. After 72-h infection, HAECs expressed dominant negative CrkI ~16–20 times more than endogeneous CrkII (Figure 4, A and B). We quantified the inhibitory effect of CrkI-R38V on membrane extension by measuring the cell size upon ephrin-B1 stimulation (Figure 4C), because membrane ruffling is associated with membrane extension and/or spreading (Lauffenburger and Horwitz, 1996). Uninfected HAECs without fluorescence showed remarkable membrane extension, whereas those infected with Adeno-CrkI-R38V

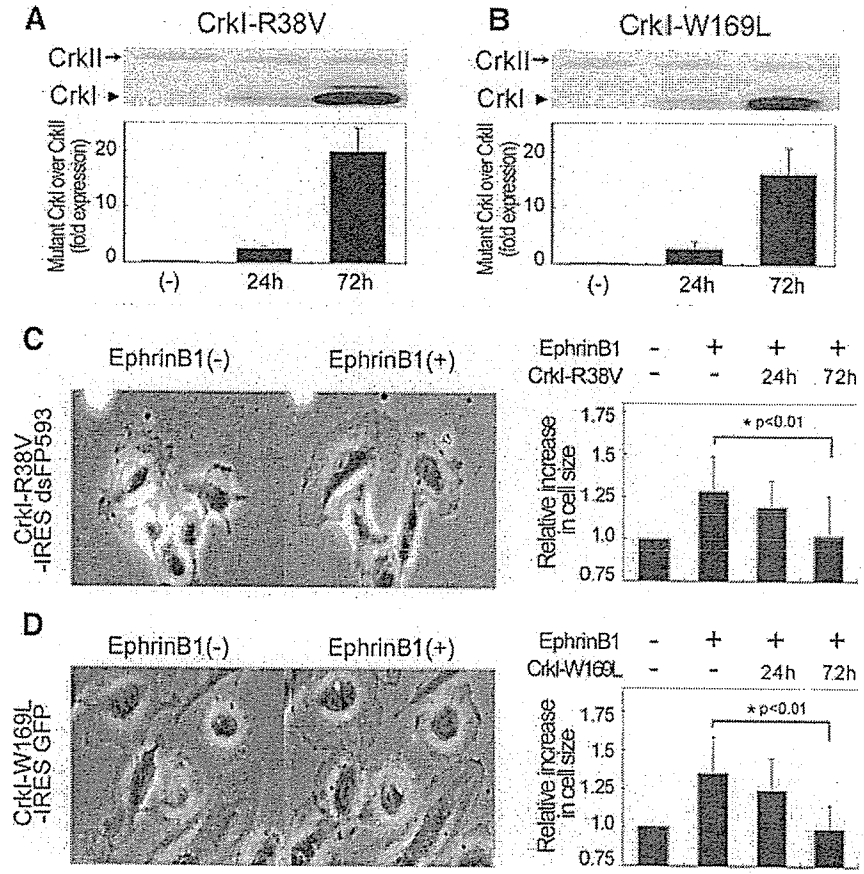

Figure 4. Crk is required for ephrin-B1–induced membrane ruffling. (A) Endogeneous CrkII and mutants of CrkI expression in HAECs infected with Adeno-CrkI-R38V for time as indicated at bottom were analyzed by immunoblotting with anti-Crk antibody (top). The quantitative analysis was performed by comparing the amount of CrkI-R38V with endogenous CrkII (bottom). (B) HAECs infected with Adeno-CrkI-W169L were similarly analyzed to CrkI-R38V. (C) Uninfected HAECs without fluorescence and HAECs infected for 72 h with Adeno-CrkI-R38V and marked by dsFP593 were cocultured, starved for 8 h, and stimulated with preclustered ephrin-B1/Fc for 30 min. Cells before and 30 min after the stimulation were imaged on an IX-70 inverted microscope (Olympus) (left). A series of time-lapse images were converted to a video. Quantitative analysis of ephrin-B1–induced membrane extension was performed by measuring the cell size of uninfected cells, those infected for 24 h, and those infected for 72 h before and after ephrin-B1 stimulation by using MetaMorph 4.6 software (right). More than 20 cells were examined in each experiment, and the results from three independent experiments have been summarized. The data are expressed as averages with the SD. A significant difference between two groups determined by *t* test is indicated with an asterisk ($P < 0.01$). (D) HAECs infected with Adeno-CrkI-W169L were similarly analyzed as shown in C. HAECs infected with Adeno-CrkI-W169L were marked by EGFP.

for 72 h and marked by IRES-driven dsFP593 did not increase their cell size (Figure 4C and Video 4A). HAECs infected for only 24 h with Adeno-CrkI-R38V responded to ephrin-B1 stimulation (Figure 4C, right). Thus, the greater the expression of CrkI-R38V, the more ephrin-B1–induced membrane extension was inhibited by CrkI-R38V. The similar inhibitory effect of CrkI-W169L on ephrin-B1–induced membrane extension was observed with CrkI-R38V (Figure 4D and Video 4B). HAECs infected with Adeno-GFP used as a negative control responded to ephrin-B1 and showed membrane ruffling, as did uninfected HAECs (our unpublished data). These results indicated that Crk SH2-binding proteins and Crk SH3-binding effectors were involved in ephrin-B1–induced membrane ruffling in HAECs.

To further confirm the requirement of Crk in ephrin-B1–induced membrane ruffling, we used RNA interference. Recently, RNA interference has become an effective strategy to knock down a target protein, not only in *C. elegans* but also in mammalian cells (Harborth *et al.*, 2001). 293T cells transfected with Crk siRNA for 72 h were depleted of Crk. Crk siRNA did not affect CrkL or actin, which were examined for the specificity of Crk siRNA (Figure 5A). Crk siRNA did inhibit the expression of CrkII in HAECs without affecting actin and β-tubulin expression (Figure 5B). The effect of Crk siRNA on ephrin-B1–induced membrane extension was examined in HAECs transfected with Crk siRNA. Because we could not distinguish HAECs that were depleted of Crk by siRNA from those untransfected, the cell number and the increase in cell size of Crk siRNA-transfected cells were compared with mock-transfected cells after ephrin-B1 stimulation. Approximately 70% of mock-treated HAECs increased their cell size >1.3 times in response to ephrin-B1 stimulation (Figure 5C, left), whereas only 30% of Crk siRNA-transfected HAECs increased (Figure 5C, right). Both the overexpression of dominant negative Crk and the depletion of Crk indicated that Crk was required for ephrin-B1–induced membrane ruffling in HAECs.

Rac1 Activation Is Required for Ephrin-B1–induced Membrane Ruffling and Subsequent Focal Complex Assembly

To examine whether Rac1, a downstream molecule of the Crk, is required for ephrin-B1–induced membrane ruffling, we transfected HAECs with dominant negative Rac1 (Rac1N17). Untransfected HAECs without fluorescence showed remarkable membrane ruffling, whereas HAEC expressing Rac1N17 marked by dsFP593 showed impaired membrane ruffling (Figure 6A and Video 6A). The inhibitory effect of Rac1N17 on membrane ruffling was again confirmed quantitatively by measuring the cell size (Figure 6B). Interestingly, we noticed that Rac1N17 also

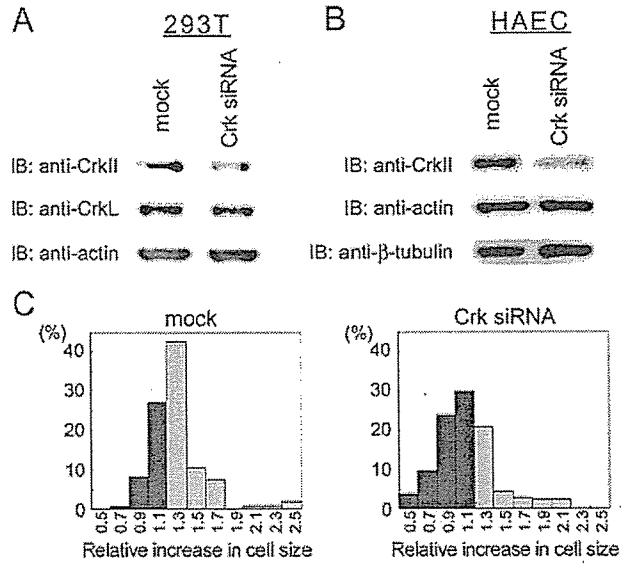

Figure 5. Depletion of Crk leads to the inhibition of ephrin-B1–induced membrane extension. (A) Mock-treated HAECs and HAECs transfected with 200 nM Crk siRNA by using OligofectAMINE for 72 h were lysed, subjected to SDS-PAGE, and immunoblotted with antibodies as indicated at the left. (B) HAECs transfected with 200 nM Crk siRNA were similarly analyzed to 293T cells. (C) Mock-treated HAECs (left) and HAECs transfected with 200 nM Crk siRNA for 72 h were analyzed for their membrane extension in response to ephrin-B1. The increase in cell size of 100 HAECs before and after ephrin-B1 stimulation was calculated as described in the legend of Figure 4.

impaired the focal complex assembly shown as the accumulation of Crk (Figure 6A, bottom and Video 6B), although this may be simply because the membrane extension must precede the focal complex assembly.

Inactivation of Rap1 Impairs Ephrin-B1–induced Focal Complex Formation

Next, we examined the role of Rap1, a downstream molecule of Crk via C3G, in ephrin-B1–induced membrane ruffling. For this, we transfected HAECs with rap1GAPII, which inactivates Rap1 by accelerating the hydrolysis of GTP (Mochizuki *et al.*, 1999). It was noteworthy that the HAECs expressing rap1GAPII marked by dsFP593 was smaller than the untransfected cells, which were without fluorescence and accentuated in the prominent peripheral focal adhesions (Figure 7A). After ephrin-B1 stimulation, membranes began ruffling in the rap1GAPII-expressing cells; however, the membrane did not extend as efficiently as did the membranes of control cells, which were without fluorescence (Figure 7A and Video 7A). We confirmed this observation by quantifying cell size (Figure 7B). This observation clearly dissociated the effect of the Crk-Rap1 pathway from that of the Crk-Rac1 pathway.

To clarify the difference between the two pathways, we analyzed the video images of rap1GAPII-expressing HAECs upon ephrin-B1 stimulation (Figure 7C and Video 7B). After stimulation, smaller and more labile focal complexes were generated at the peripheral region. Some peripheral focal adhesions were observed to detach from the substratum and move toward the center of the cell (Video 7B). This observation suggested that Rap1 was required for the stabilization of focal complexes, which followed the membrane spreading in normal HAECs.

Rap1 Is Activated at the Membrane Ruffling upon Ephrin-B1 Stimulation

Previously, we showed that epidermal growth factor stimulated Ras at the periphery and Rap1 at the center of cells. Because the requirement of Rap1 in the membrane spreading seemed to contradict this previous observation, we examined the spatiotemporal pattern of the activation of Rap1 and Ras. The principle of the monitors for Ras-family G proteins named Raichu is illustrated in Figure 8A. These

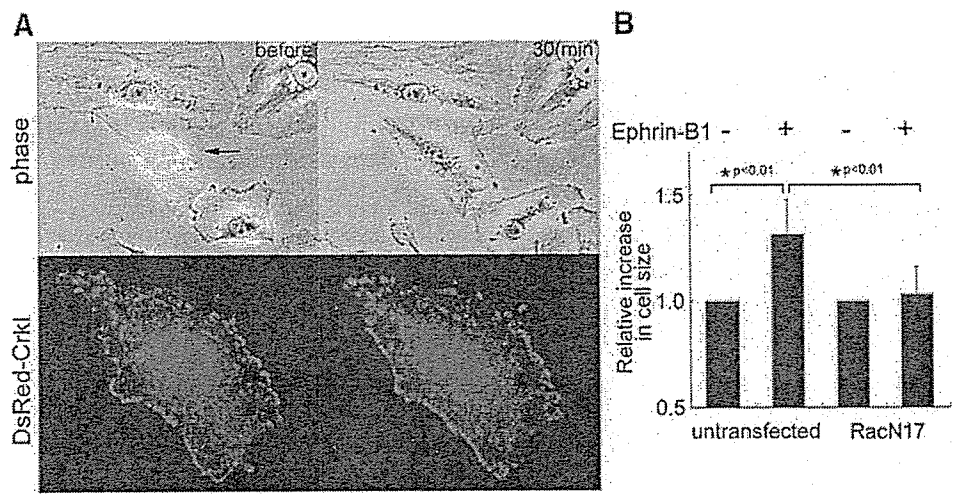

Figure 6. Rac1 activation is essential for ephrin-B1–induced membrane ruffling. (A) HAECs transfected with pCXN2-FLAG-Rac1N17-IRES-EGFP and pCA-DsRed-CrkI were stimulated with preclustered ephrin-B1/Fc. Epifluorescent images of both EGFP and DsRed were overlaid on phase-contrast view before the stimulation (top left). The representative phase-contrast images before and after stimulation are shown (top). DsRed image of the cell expressing Rac1N17 and DsRed-CrkI indicated by the arrow was enlarged before (bottom left) and after (bottom right) the stimulation. (B) Effect of Rac1N17 on ephrin-B1–induced membrane extension was analyzed as in Figure 4. A significant difference between two groups determined by *t* test is indicated with an asterisk ($P < 0.01$).

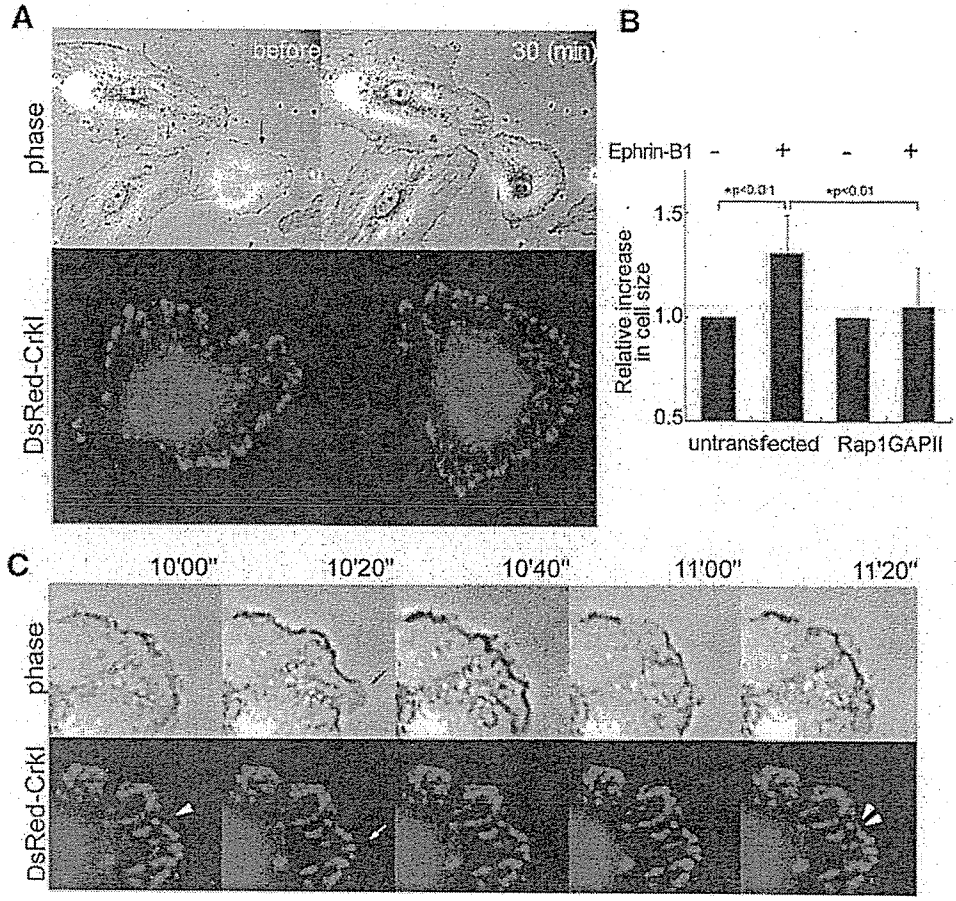

Figure 7. Inhibition of Rap1 by overexpression of rap1GAPII suppresses focal complex assembly and maturation. (A) HAECs transfected with pCXN2-FLAG-rap1GAPII-IRES-EGFP and pCA-DsRed-CrkI were stimulated with preclustered ephrin-B1/Fc. Epifluorescent images of EGFP and DsRed were overlaid on the phase-contrast image before the stimulation (top left). Representative images before and 30 min after ephrin-B1 stimulation are shown. DsRed image of the cell expressing both rap1GAPII and DsRed-CrkI (indicated by arrow) was enlarged to show focal complex formation (bottom). (B) Effect of rap1GAPII on membrane extension was analyzed as described in the legend of Figure 4. A significant difference between two groups determined by *t* test is indicated with an asterisk ($P < 0.01$). (C) A series of closer views of phase contrast and DsRed images of the cell shown in A. Images were obtained at the time after stimulation, as indicated at the top. The arrows indicate ruffled membrane without focal complex formation. Note labile focal complexes indicated by the double arrowheads. The single arrowhead indicates where labile focal complex are generated (also see Video 6B).

probes consisted of YFP, Ras, Raf, and CFP, and the CAAX box of Ki-Ras. In its inactive form, only fluorescence from CFP can be detected. On the activation of Ras and succeeding binding to Raf, excited CFP transfers its energy to YFP, resulting in the emanation of yellow fluorescence. By measuring the fluorescence ratio of YFP/CFP, we can measure the activity of Ras.

HAECs were infected with Adeno-Raichu-Rap1 or Ras. The basal Rap1 activity was high at the perinuclear region, as we have previously reported in COS-1 cells (Figure 8B, top, and Video 8). On ephrin-B1 stimulation, Rap1 was rapidly activated at the membrane ruffling and it continued for ~15 min. In contrast to Rap1, Ras activity was decreased by ephrin-B1 stimulation. The Ras activity reached its lowest level within 5 min after the stimulation. The inactivation of Ras continued for >30 min (Figure 8B, bottom). These results showed for the first time Rap1 activation at the membrane ruffling. Because Rap1 is known to antagonize Ras-induced extracellular signal-regulated kinase activation, this anticorrelation of the activity may be another example of the anti-Ras function of Rap1. In addition, we tested whether the Rap1 activation upon ephrin-B1 stimulation was dependent on Crk. HAECs expressing Raichu-Rap1 showed Rap1 activation at the membrane ruffling as shown in Figure 8B, whereas HAECs expressing Raichu-Rap1 and CrkI-R38V, which sequestered Crk SH3-binding proteins, did not exhibit any Rap1 activation and membrane extension (Figure 8C). CrkI-R38V did not inhibit ephrin-B1–induced inactivation of Ras (our unpublished data). These results indicated that Crk was required for the activation of Rap1 upon ephrin-B1 stimulation in HAECs.

DISCUSSION

Eph/ephrin-induced reciprocal signaling pathway has been implicated in the repulsive force produced by the cells expressing EphB and those expressing ephrin on their cell surface. This reciprocal signal from either Eph or ephrin plays critical roles in embryogenesis, rhombomere segmentation, axonal guidance, neural crest cell migration, and vasculogenesis (Holder and Klein, 1999). Furthermore, in angiogenesis, sprouting and subsequent migration of endothelial cells is thought to be promoted by ephrin/Eph engagement-dependent repulsive force between endothelial cells and/or their surrounding mesenchymal cells. However, how the repulsion mechanism is promoted in vascular endothelial cells remains elusive.

We have shown herein that the Rac1 activation is required for ephrin-B1–induced initial membrane spreading, based on the finding that the dominant negative form of Rac1 suppressed the initial membrane spreading (Figure 6). It has

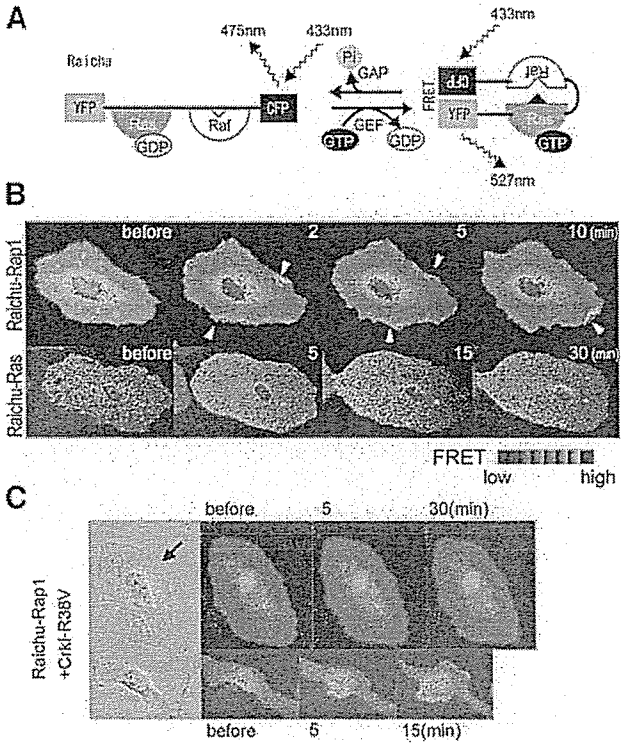

Figure 8. Activation of Rap1 at the membrane ruffling and inactivation of Ras upon ephrin-B1 stimulation in HAECs. (A) Schematic representation of Raichu-Ras. FRET efficiency in a manner dependent on the bound guanine nucleotides. 433 nm, excitation for CFP; 475 nm, emission from CFP; 527 nm, emission from YFP due to FRET; Ras, H-Ras; Raf, Ras-binding domain of Raf. (B) HAECs infected with Adeno-Raichu-Rap1 (top) or Raichu-Ras (bottom) were starved for 8 h and stimulated with 1 μg/ml preclustered ephrin-B1/Fc for the time indicated at the top. Arrowheads indicate membrane ruffles. The red hue and blue hue indicate an increase (high) and a decrease (low) in the ratio of YFP to CFP, respectively, reflecting FRET efficiency. (C) HAECs infected with Adeno-Raichu-Rap1 for 48 h and Adeno-CrkI-R38V for 72 h (arrow) and those infected only with Adeno-Raichu-Rap1 were cocultured, straved, and stimulated with preclustered ephrin-B1/Fc for time period as indicated at the top. Phase contrast image before the stimulation was overlaid onto the image for dsFP593 to distinguish HAECs infected with Adeno-CrkI-R38V from those infected only with Adeno-Raichu-Rap1. FRET images were obtained every 20 s.

been demonstrated that a Crk-binding protein, DOCK180, can bind to and activate Rac1 (Kiyokawa *et al.*, 1998). Cheresh *et al.* (1999) showed that the Crk-DOCK180-Rac1 pathway plays an essential role in the cell migration of fibroblasts. The requirement of Crk for Rac1 activation, as assessed by initial membrane spreading, is evidenced by the findings that both the overexpression of CrkI-R38V and the depletion of Crk by siRNA inhibited the membrane extension upon ephrin-B1 stimulation (Figures 4C and 5). Thus, ephrin-B1 probably activates Rac1 via Crk-DOCK180.

Previous reports have demonstrated that Rap1 is required for integrin-mediated cell adhesion (Caron *et al.*, 2000; Reedquist *et al.*, 2000) and that C3G, another Crk-binding protein, mediates Rap1 activation in this process (Ohba *et al.*, 2001). In this report, we have shown that Rap1 activation is essential for the assembly and maturation of focal complexes in HAECs stimulated with ephrin-B1. Li *et al.* (2002) have recently shown that the C3G-activated Rap1 stabilizes focal adhesions. Thus, the attachment of the ruffled membrane to ECM via integrin may require Rap1 activation. This notion is supported by the fact that overexpression of rap1GAPII inhibited the focal complex formation (Figure 7 and Video 7B) and also by the finding that Rap1 was indeed activated at the membrane ruffling, upon ephrin-B1 stimulation (Figure 8 and Video 8). In addition, Rap1 activation was inhibited by CrkI-R38V, implicating Crk SH3-binding proteins in ephrin-B1–induced Rap1 activation (Figure 8C). Among Crk SH3-binding molecules, C3G is the only guanine nucleotide exchange factor (GEF) for Rap1 (Kiyokawa *et al.*, 1997). In accordance with this, our results suggest that the Crk-C3G-Rap1 pathway may be involved in the stability and maturation of focal complexes. Further study is needed to identify the effector molecules of Rap1 in the stabilization of focal complexes.

We revealed that Crk colocalized with $p130^{Cas}$ at the nascent focal complexes in ephrin-B1–stimulated HAECs. Crk-$p130^{Cas}$ complex plays a pivotal role in cell migration through DOCK180 and Rac1 (Klemke *et al.*, 1998; Cheresh *et al.*, 1999). Furthermore, the activation of Src kinase promotes $p130^{Cas}$ association with Crk and C3G to activate Rap1 (Xing *et al.*, 2000). Thus, the Crk-$p130^{Cas}$ complex might activate both Rac1 and Rap1 at the focal complexes. Previously, paxillin, another SH2-binding protein of Crk at cell adhesions, was shown to counteract $p130^{Cas}$ in cell migration (Yano *et al.*, 2000). Therefore, transition from Crk-paxillin to Crk-$p130^{Cas}$ upon ephrin-B1 stimulation may be preferable for cell migration.

By the use of FRET technology, we have shown for the first time that Rap1 is activated at membrane ruffles in response to ephrin-B1 stimulation, whereas Ras is inactivated in HAECs.

Previously, we demonstrated that epidermal growth factor induces Ras activation in the membrane ruffling and Rap1 activation in the perinuclear region of COS-1 cells (Mochizuki *et al.*, 2001). Rap1 and Ras antagonize each other in cell transformation and extracellular signal-regulated kinase activation (Kitayama *et al.*, 1989; Cook *et al.*, 1993). This notion is consistent with the different spatial activation of Rap1 and Ras in COS-1 cells and the activation of Rap1 and the inactivation of Ras in ephrin-B1–stimulated HAECs.

Ras is inactivated upon EphA2-activation by ephrin-A1 in human prostatic epithelial cells, and bovine aortic endothelial cells (Miao *et al.*, 2001). p120-RasGAP, a GTPase-activating protein (GAP) for Ras, binds to EphB2 in neuronal NG108 cells and participates in the down-regulation of Ras upon EphB2 activation by ephrin-B1 (Elowe *et al.*, 2001). Thus, p120-RasGAP may be involved in ephrin-B1–induced inactivation of Ras in HAECs.

We have demonstrated that Crk is required for Rap1 activation (Figure 8C). SHEP1 is considered to be a signaling intermediator that binds EphB2 via its SH2 and Rap1 via the GEF domain (Dodelet *et al.*, 1999), although its function has not been clearly demonstrated yet. Chat, a shorter splicing variant of SHEP, is isolated as a $p130^{Cas}$/HEF1-associated adaptor (Sakakibara and Hattori, 2000). Thus, Chat may connect EphB to $p130^{Cas}$-Crk and its SH3-binding proteins,

C3G, to activate Rap1. Accordingly, stimulation-dependent translocation of GEFs and GAPs regulated by adaptor and/or docking proteins, including Crk, p130^{Cas}, and p120-RasGAP may account for exclusive activation of Ras and Rap1.

In conclusion, we have demonstrated that Crk is required for cooperative activation of Rac1 and Rap1 to promote cell migration by inducing membrane ruffling and stabilizing focal complexes.

ACKNOWLEDGMENTS

We thank A. Miyawaki for the plasmids; H. Kuorse for the virus; B. J. Mayer for the cells; M. Sone, and H. Shimamoto for their technical assistance. This work was supported in part by grants from the Ministry of Health, Labor and Welfare Foundation of Japan, from the Promotion of Fundamental Studies in Health Science of the Organization for Pharmaceutical Safety and Research of Japan, from the Human Science Foundation of Japan, and from Yamanouchi Foundation for Research on Metabolic Disorders, as well as by an Astra Zeneca Research Grant.

REFERENCES

Bar-Sagi, D., and Hall, A. (2000). Ras, and Rho GTPases. a family reunion. Cell *103*, 227–238.

Birge, R.B., Fajardo, J.E., Reichman, C., Shoelson, S.E., Songyang, Z., Cantley, L.C., and Hanafusa, H. (1993). Identification and characterization of a high-affinity interaction between v-Crk and tyrosine-phosphorylated paxillin in CT10-transformed fibroblasts. Mol. Cell. Biol. *13*, 4648–4656.

Brückner, K., Pasquale, E.B., and Klein, R. (1997). Tyrosine phosphorylation of transmembrane ligands for Eph receptors. Science *275*, 1640–1643.

Carmeliet, P., and Jain, R.K. (2000). Angiogenesis in cancer and other diseases. Nature *407*, 249–257.

Caron, E., Self, A.J., and Hall, A. (2000). The GTPase Rap1 controls functional activation of macrophage integrin $\alpha_M\beta_2$ by LPS and other inflammatory mediators. Curr. Biol. *10*, 974–978.

Cheresh, D.A., Leng, J., and Klemke, R.L. (1999). Regulation of cell contraction and membrane ruffling by distinct signals in migratory cells. J. Cell Biol. *146*, 1107–1116.

Cook, S.J., Rubinfeld, B., Albert, I., and McCormick, F. (1993). RapV12 antagonizes Ras-dependent activation of ERK1 and ERK2 by LPA and EGF in Rat-1 fibroblasts. EMBO J. *12*, 3475–3485.

Cowan, C.A., and Henkemeyer, M. (2001). The SH2/SH3 adaptor Grb4 transduces B-ephrin reverse signals. Nature *413*, 174–179.

Dodelet, V.C., and Pasquale, E.B. (2000). Eph receptors and ephrin ligands: embryogenesis to tumorigenesis. Oncogene *19*, 5614–5619.

Dodelet, V.C., Pazzagli, C., Zisch, A.H., Hauser, C.A., and Pasquale, E.B. (1999). A novel signaling intermediate, SHEP1, directly couples Eph receptors to R-Ras and Rap1A. J. Biol. Chem. *274*, 31941–31946.

Elowe, S., Holland, S.J., Kulkarni, S., and Pawson, T. (2001). Down-regulation of the Ras-mitogen-activated protein kinase pathway by the EphB2 receptor tyrosine kinase is required for ephrin-induced neurite retraction. Mol. Cell. Biol. *21*, 7429–7441.

Endo, A., Nagashima, K., Kurose, H., Mochizuki S., Matsuda, M., and Mochizuki, N. (2002). Sphingosine 1-phosphate induces membrane ruffling and increases motility of human umbilical vein endothelial cells via vascular endothelial growth factor receptor and CrkII. J. Biol. Chem. 277, 23747–23754.

Eph Nomenclature Committee. (1997). Unified nomenclature for Eph family receptors and their ligands, the ephrins. Eph Nomenclature Committee letter. Cell *90*, 403–404.

Erickson, M.R., Galletta, B.J., and Abmayr, S.M. (1997). *Drosophila* myoblast city encodes a conserved protein that is essential for myoblast fusion, dorsal closure, and cytoskeletal organization. J. Cell Biol. *138*, 589–603.

Fradkov, A.F., Chen, Y., Ding, L., Barsova, E.V., Matz, M.V., and Lukyanov, S.A. (2000). Novel fluorescent protein from *Discosoma* coral and its mutants possesses a unique far-red fluorescence. FEBS Lett. *479*, 127–130.

Gale, N.W., Baluk, P., Pan, L., Kwan, M., Holash, J., DeChiara, T.M., McDonald, D.M., and Yancopoulos, G.D. (2001). Ephrin-B2 selectively marks arterial vessels and neovascularization sites in the adult, with expression in both endothelial and smooth-muscle cells. Dev. Biol. *230*, 151–160.

Geiger, B., Bershadsky, A., Pankov, R., and Yamada, K.M. (2001). Transmembrane crosstalk between the extracellular matrix-cytoskeleton crosstalk. Nat. Rev. Mol. Cell. Biol. *2*, 793–805.

Harborth, J., Elbashir, S.M., Bechert, K., Tuschl, T., and Weber, K. (2001). Identification of essential genes in cultured mammalian cells using small interfering RNAs. J. Cell Sci. *114*, 4557–4565.

Hock, B., Böhme, B., Karn, T., Feller, S., Rübsamen-Waigmann, H., and Strebhardt, K. (1998). Tyrosine-614, the major autophosphorylation site of the receptor tyrosine kinase HEK2, functions as multidocking site for SH2-domain mediated interactions. Oncogene *17*, 255–260.

Holder, N., and Klein R. (1999). Eph receptors and ephrins: effectors of morphogenesis. Development *126*, 2033–2044.

Ichiba, T., Hashimoto, Y., Nakaya, M., Kuraishi, Y., Tanaka, S., Kurata, T., Mochizuki, N., and Matsuda, M. (1999). Activation of C3G guanine nucleotide exchange factor for Rap1 by phosphorylation of tyrosine 504. J. Biol. Chem. *274*, 14376–14381.

Ichiba, T., Kuraishi, Y., Sakai, O., Nagata, S., Groffen, J., Kurata, T., Hattori, S., and Matsuda, M. (1997). Enhancement of guanine-nucleotide exchange activity of C3G for Rap1 by the expression of Crk, CrkL, and Grb2. J. Biol.Chem. *272*, 22215–22220.

Kitayama, H., Sugimoto, Y., Matsuzaki, T., Ikawa, Y., and Noda, M. (1989). A ras-related gene with transformation suppressor activity. Cell *56*, 77–84.

Kiyokawa, E., Hashimoto, Y., Kobayashi, S., Sugimura, H., Kurata, T., and Matsuda, M. (1998). Activation of Rac1 by a Crk SH3-binding protein, DOCK180. Genes Dev. *12*, 3331–3336.

Kiyokawa, E., Mochizuki, N., Kurata, T., and Matsuda, M. (1997). Role of Crk oncogene product in physiologic signaling. Crit. Rev. Oncog. *8*, 329–342.

Klemke, R.L., Leng, J., Molander, R., Brooks, P.C., Vuori, K., and Cheresh, D.A. (1998). CAS/Crk coupling serves as a "molecular switch" for induction of cell migration. J. Cell Biol. *140*, 961–972.

Lauffenburger, D.A., and Horwitz, A.F. (1996). Cell migration: a physically integrated molecular process. Cell *84*, 359–369.

Li, L., Okura, M., and Imamoto, A. (2002). Focal adhesions require catalytic activity of SRC family kinases to mediate integrin-matrix adhesion. Mol. Cell. Biol. *22*, 1203–1217.

Lu, Q., Sun, E.E., Klein, R.S., and Flanagan, J.G. (2001). Ephrin-B reverse signaling is mediated by a novel PDZ-RGS protein and selectively inhibits G protein-coupled chemoattraction. Cell *105*, 69–79.

Matsuda, M., Tanaka, S., Nagata, S., Kojima, A., Kurata, T., and Shibuya, M. (1992). Two species of human CRK cDNA encode proteins with distinct biological activities. Mol. Cell. Biol. *12*, 3482–3489.

Miao, H., Wei, B., Peehl, D.M., Li, Q., Alexandrou, T., Schelling, J.R., Rhim, J.S., Sedor, J.R., Burnett, E., and Wang, B. (2001). Activation of EphA receptor tyrosine kinase inhibits the Ras/MAPK pathway. Nat. Cell. Biol. *3*, 527–530.

Mochizuki, N., Ohba, Y., Kiyokawa, E., Kurata, T., Murakami, T., Ozaki, T., Kitabatake, A., Nagashima, K., and Matsuda, M. (1999). Activation of the ERK/MAPK pathway by an isoform of rap1GAP associated with Gαi. Nature *400*, 891–894.

Mochizuki, N., Yamashita, S., Kurokawa, K., Ohba, Y., Nagai, T., Miyawaki, A., and Matsuda, M. (2001). Spatio-temporal images of growth-factor-induced activation of Ras and Rap1. Nature *411*, 1065–1068.

Niwa, H., Yamamura, K., and Miyazaki, J. (1991). Efficient selection for high-expression transfectants with a novel eukaryotic vector. Gene *108*, 193–199.

Ohba, Y., *et al.* (2001). Requirement for C3G-dependent Rap1 activation for cell adhesion and embryogenesis. EMBO J. *20*, 3333–3341.

Reddien, P.W., and Horvitz, H.R. (2000). CED-2/CrkII and CED-10/Rac control phagocytosis and cell migration in *Caenorhabditis elegans*. Nat. Cell Biol. *2*, 131–136.

Reedquist, K.A., Ross, E., Koop, E.A., Wolthuis, R.M., Zwartkruis, F.J., van Kooyk, Y., Salmon, M., Buckley, C.D., and Bos, J.L. (2000). The small GTPase, Rap1, mediates CD31-induced integrin adhesion. J. Cell Biol. *148*, 1151–1158.

Risau, W. (1997). Mechanisms of angiogenesis. Nature *386*, 671–674.

Rottner, K., Hall, A., and Small, J.V. (1999). Interplay between Rac and Rho in the control of substrate contact dynamics. Curr. Biol. *9*, 640–648.

Sakai, R., Iwamatsu, A., Hirano, N., Ogawa, S., Tanaka, T., Mano, H., Yazaki, Y., and Hirai, H. (1994). A novel signaling molecule, p130, forms stable complexes in vivo with v-Crk and v-Src in a tyrosine phosphorylation-dependent manner. EMBO J. *13*, 3748–3756.

Sakakibara, A., and Hattori, S. (2000) Chat, a Cas/HEF-associated adaptor protein that integrates multiple signaling pathways. J. Biol. Chem. *275*, 6404–6410.

Schaller, M.D., and Parsons, J.T. (1995). pp125FAK-dependent tyrosine phosphorylation of paxillin creates a high-affinity binding site for Crk. Mol. Cell. Biol. *15*, 2635–2645.

Shin, D., Garcia-Cardena, G., Hayashi, S., Gerety, S., Asahara, T., Stavrakis, G., Isner, J., Folkman, J., Gimbrone, Jr., M.A., and Anderson, D.J. (2001). Expression of ephrinB2 identifies a stable genetic difference between arterial and venous vascular smooth muscle as well as endothelial cells, and marks subsets of microvessels at sites of adult neovascularization. Dev. Biol. *230*, 139–150.

Stein, E., Cerretti, D.P., and Daniel, T.O. (1996). Ligand activation of ELK receptor tyrosine kinase promotes its association with Grb10 and Grb2 in vascular endothelial cells. J. Biol. Chem. *271*, 23588–23593.

Vuori, K., Hirai, H., Aizawa, S., and Ruoslahti, E. (1996). Introduction of p130cas signaling complex formation upon integrin-mediated cell adhesion: a role for Src family kinases. Mol. Cell. Biol. *16*, 2606–2613.

Wang, H.U., Chen, Z.F., and Anderson, D.J. (1998). Molecular distinction and angiogenic interaction between embryonic arteries and veins revealed by ephrin-B2 and its receptor Eph-B4. Cell *93*, 741–753.

Wu, Y.C., and Horvitz, H.R. (1998). *C. elegans* phagocytosis and cell-migration protein CED-5 is similar to human DOCK180. Nature *392*, 501–504.

Xing, L., Ge, C., Zeltser, R., Maskevitch, G., Mayer, B.J., and Alexandropoulos, K. (2000). c-Src signaling induced by the adapters Sin, and Cas is mediated by Rap1 GTPase. Mol. Cell Biol. *20*, 7363–7377.

Yancopoulos, G.D., Davis, S., Gale, N.W., Rudge, J.S., Wiegand, S.J., and Holash, J. (2000). Vascular-specific growth factors and blood vessel formation. Nature *407*, 242–248.

Yancopoulos, G.D., Klagsbrun, M., and Folkman, J. (1998). Vasculogenesis, angiogenesis, and growth factors: ephrins enter the fray at the border. Cell *93*, 661–664.

Yano, H., Uchida, H., Iwasaki, T., Mukai, M., Akedo, H., Nakamura, K., Hashimoto, S., and Sabe, H. (2000). Paxillin alpha and Crk-associated substrate exert opposing effects on cell migration and contact inhibition of growth through tyrosine phosphorylation. Proc. Natl. Acad. Sci. USA *97*, 9076–9081.

Yu, H.H., Zisch, A.H., Dodelet, V.C., and Pasquale, E.B. (2001). Multiple signaling interactions of Abl and Arg kinases with the EphB2 receptor. Oncogene *20*, 3995–4006.

Zisch, A.H., Pazzagli, C., Freeman, A.L., Schneller, M., Hadman, M., Smith, J.W., Ruoslahti, E., and Pasquale, E.B. (2000). Replacing two conserved tyrosines of the EphB2 receptor with glutamic acid prevents binding of SH2 domains without abrogating kinase activity and biological responses. Oncogene *19*, 177–187.

Journal of the American College of Cardiology
© 2002 by the American College of Cardiology Foundation
Published by Elsevier Science Inc.

Vol. 40, No. 5, 2002
ISSN 0735-1097/02/$22.00
PII S0735-1097(02)02056-9

Amelioration of Ischemia- and Reperfusion-Induced Myocardial Injury by the Selective Estrogen Receptor Modulator, Raloxifene, in the Canine Heart

Hisakazu Ogita, MD,* Koichi Node, MD,* Hiroshi Asanuma, MD,* Shoji Sanada, MD,* Yulin Liao, MD,* Seiji Takashima, MD,* Masanori Asakura, MD,* Hidezo Mori, MD,§ Yoshiro Shinozaki, MD,† Masatsugu Hori, MD, FACC,* Masafumi Kitakaze, MD, FACC‡

Osaka, Japan

OBJECTIVES We sought to investigate whether raloxifene reduces ischemia-reperfusion injury and what mechanisms are involved in the cardioprotective effects.

BACKGROUND Estradiol-17-beta reduces myocardial infarct size in ischemia-reperfusion injury. Raloxifene, a selective estrogen receptor modulator, demonstrates immediate coronary artery vasorelaxing effects.

METHODS The myocardial ischemia-reperfusion model included anesthetized open-chest dogs after 90-min occlusion of the left anterior descending coronary artery (LAD) and subsequent 6-h reperfusion. Raloxifene and/or other drugs were infused into the LAD from 10 min before coronary occlusion to 1 h after reperfusion without an occlusion period.

RESULTS Infarct size was reduced in the raloxifene (5 μg/kg per min) group compared with the control group (7.2 ± 2.5% vs. 40.9 ± 3.9% of the area at risk, $p < 0.01$). Either N^G-nitro-L-arginine methyl ester (L-NAME), the inhibitor of nitric oxide (NO) synthase, or charybdotoxin, the blocker of Ca^{2+}-activated K^+ (K_{Ca}) channels, partially attenuated the infarct size–limiting effect, and both of them completely abolished the effect. The incidence of ventricular fibrillation was also less in the raloxifene group than in the control group (11% vs. 44%, $p < 0.05$). Activity of p38 mitogen-activated protein (MAP) kinase increased with 15-min ischemia, and raloxifene pretreatment inhibited the activity. Myeloperoxidase activity of the 6-h reperfused myocardium was also attenuated by raloxifene.

CONCLUSIONS These data demonstrate that raloxifene reduces myocardial ischemia-reperfusion injury by mechanisms dependent on NO and the opening of K_{Ca} channels in canine hearts. Deactivation of p38 MAP kinase and myeloperoxidase by raloxifene may be involved in the cellular mechanisms of cardioprotection. (J Am Coll Cardiol 2002;40:998–1005) © 2002 by the American College of Cardiology Foundation

Estrogen replacement therapy may reduce cardiovascular events in postmenopausal women (1). We have previously demonstrated that estradiol-17-beta reduced the myocardial infarct (MI) size and the occurrence of ischemia- and reperfusion-induced ventricular arrhythmias (2) and that it increased coronary blood flow in canine ischemic hearts (3). These effects are mediated by both estrogen-induced enhancement of nitric oxide (NO) production and the probability of open Ca^{2+}-activated K^+ (K_{Ca}) channels. Despite these beneficial effects, estrogen replacement therapy appears to increase the risk of endometrial or breast cancer and may be associated with an increased risk of venous thromboembolism (4,5). Raloxifene, one of the selective estrogen receptor modulators, exerts estrogenic agonistic or antagonistic actions on different tissues and has been recently introduced as a drug for new hormone replacement therapy because of the reduced adverse effects of estrogen. It prevents bone loss and has lipid-lowering effects in humans (6–10). Although it also exhibits coronary-relaxing effects on the coronary artery in vitro (11), it remains unclear whether raloxifene has beneficial effects during ischemia and reperfusion in vivo. If raloxifene does not mediate cardioprotection, as estradiol-17-beta does, the rationale for the use of raloxifene as hormone replacement therapy may be weakened.

Therefore, we investigated the effects of raloxifene on MI size and the occurrence of ischemia- and reperfusion-induced ventricular arrhythmias. We infused raloxifene into the coronary artery of open-chest dogs and also examined whether the effects are involved in NO or the opening of K_{Ca} channels. Furthermore, we also examined the activities of three major mitogen-activated protein (MAP) kinases—p38 MAP kinase, c-Jun NH_2-terminal protein kinase (JNK) and extracellular signal–regulated protein kinase (ERK)—during ischemia, because these MAP kinases are known to be the mechanism of cellular signaling for cardiac injury and protection (12–16).

METHODS

Instrumentation. Seventy-four beagle dogs weighing 8 to 12 kg were anesthetized with intravenous sodium pentobar-

From the *Department of Internal Medicine and Therapeutics, Osaka University Graduate School of Medicine, Suita; †Department of Physiological Science, Tokai University School of Medicine, Isehara; and ‡Cardiovascular Division of Medicine and the §Department of Cardiac Physiology, National Cardiovascular Center, Suita, Japan. This study was partially supported by Comprehensive Research on Aging and Health, Ministry of Health and Welfare, Grants-in-Aid for Scientific Research (nos. 12470153 and 12877107) for the Ministry of Education, Culture, Sports, Science and Technology and by the Smoking Research Foundation in Japan.

Manuscript received April 30, 2001; revised manuscript received April 29, 2002, accepted May 24, 2002.

Abbreviations and Acronyms

CTX	= charybdotoxin
ERK	= extracellular signal–regulated protein kinase
JNK	= *c*-Jun NH_2-terminal protein kinase
K_{Ca}	= Ca^{2+}-activated K^+
LAD	= left anterior descending coronary artery
L-NAME	= N^G-nitro-L-arginine methyl ester
MAP	= mitogen-activated protein
MBP	= myelin basic protein
MI	= myocardial infarct
MPO	= myeloperoxidase
NO	= nitric oxide

bital (30 mg/kg), intubated with a cuffed endotracheal tube and ventilated with room air mixed with oxygen (1.5 l/min) with the use of a respirator. Intravenous infusion of sodium pentobarbital (approximately 30 mg/h) was continued during the experimental protocol to maintain hemodynamic stabilization. The method of preparation for the experiments of ischemia-reperfusion injury in the canine heart was previously described (2). Briefly, the left anterior descending coronary artery (LAD) was cannulated and perfused with blood through an extracorporeal tube from the left carotid artery. The femoral artery and left atrium were cannulated to obtain a reference blood flow sample for calculation of the regional myocardial blood flow and to inject microspheres, respectively. Heparin (500 U/kg) was administered intravenously every 3 h throughout the protocol. All studies conformed with the position of the National Institutes of Health (NIH), in its Guide for the Care and Use of Laboratory Animals, adopted in November 1984.

Experimental protocols. PROTOCOL 1: EFFECTS OF RALOXIFENE ON INFARCT SIZE AND ISCHEMIA- AND REPERFUSION-INDUCED VENTRICULAR ARRHYTHMIAS. After hemodynamic stabilization, infusion of raloxifene (0.5 or 5 μg/kg per min; Eli Lilly, Indianapolis, Indiana), vehicle (0.1% [vol/vol] dimethyl sulfoxide) or saline (control group) was initiated into the bypass tube 10 min before coronary occlusion and continued until 1 h after reperfusion without the occlusion period (control group: n = 9; vehicle group: n = 9; raloxifene groups: 0.5 μg/kg per min, n = 6 and 5 μg/kg per min, n = 9). The intracoronary infusion of 5 μg/kg per min of raloxifene theoretically corresponded to 1 μmol/l in the coronary artery blood, which was shown in a previous study to maximally relax the coronary arteries (11), and 0.5 μg/kg per min of raloxifene was also infused to examine the dose-dependent effects of raloxifene.

In 10-min infusion, the coronary artery was occluded for 90 min and then reperfused for 6 h. Hemodynamic variables were measured before the administration of drugs and sustained ischemia at 10 and 90 min after the onset of ischemia and at 1, 3, and 6 h after the onset of reperfusion.

PROTOCOL 2: ROLE OF NO AND KCA CHANNELS IN RALOXIFENE-INDUCED ATTENUATION OF INFARCT SIZE AND INCIDENCE OF ISCHEMIA- AND REPERFUSION-INDUCED VENTRICULAR ARRHYTHMIAS. The effects of raloxifene were examined in dogs pretreated with N^G-nitro-L-arginine methyl ester (L-NAME, an inhibitor of NO synthase) or charybdotoxin (CTX, a blocker of K_{Ca} channels). Infusion of either L-NAME (10 μg/kg per min; Sigma) or CTX (1 μg/kg per min; Sigma, St. Louis, Missouri) into the bypass tube was initiated 10 min before infusion of raloxifene (5 μg/kg per min) and continued until 1 h of reperfusion after the 90-min occlusion period (raloxifene + L-NAME group, n = 7; raloxifene + CTX group, n = 7; raloxifene + L-NAME + CTX group, n = 7). To examine the effects of inhibitors of ischemia-reperfusion injury, we also infused only L-NAME and CTX (n = 8) into the bypass tube during the same period as described earlier. The dose of L-NAME completely abolished the release of NO (17), and the dose of CTX also maximally attenuated bradykinin-induced coronary vasodilation (18). Hemodynamic variables were measured at the same time as in protocol 1.

PROTOCOL 3: EFFECTS OF RALOXIFENE ON MAP KINASE ACTIVITY DURING ISCHEMIA. We used 12 dogs in this protocol and classified them into four groups: no ischemia, ischemia, 10-min pretreatment with raloxifene before ischemia and 10-min pretreatment with raloxifene, L-NAME and CTX before ischemia. In the group with no ischemia, the LAD of three dogs was cannulated and perfused with blood through a bypass tube for 25 min. In the group with ischemia, the tube was occluded for 15 min after 10 min of hemodynamic stabilization, and in the group with raloxifene pretreatment or raloxifene plus inhibitors pretreatment before ischemia, 10-min infusion of raloxifene with or without L-NAME and CTX into the LAD was performed before 15 min of complete coronary artery occlusion. After these procedures were done, we sacrificed the dogs, excised the hearts and quickly sampled myocardial tissue supplied by the LAD into liquid nitrogen and stored −80°C.

Criteria for exclusion. To ensure that all of the animals included in the analysis of infarct size data were healthy and exposed to similar degrees of ischemia, we adopted the following criteria for the exclusion of unsatisfactory dogs: 1) subendocardial collateral flow >15 ml/100 g per min; 2) heart rate >170 beats/min; or 3) more than two consecutive attempts required to correct ventricular fibrillation (VF) with low-energy, direct-current pulses applied directly to the heart. We calculated the survival percentage as the number of dogs that survived/number of assigned dogs × 100.

Measurement of infarct size and regional myocardial blood flow. We measured infarct size as previously described (2). Briefly, after 6 h of reperfusion, we re-occluded the LAD and injected Evans' blue dye into a systemic vein. Then, the sliced LAD was incubated in 1% 2,3,5-Triphenyltetrazolium chloride (Sigma) solution to detect the

JACC Vol. 40, No. 5, 2002
September 4, 2002:998–1005

Table 1. Number of Dogs Assigned to and Excluded From Each Group for Measurement of Infarct Size

	Dogs Originally Assigned (n)	Dogs Used for Data Analysis (n)	Reason for Exclusion		
			VF (>2) During 6 h Reperfusion (n)	Death Due to VF (n)	High Collateral Blood Flow (>15 ml/100 g per min)
Saline	9	7	1	1	0
Vehicle	9	7	1	0	1
Raloxifene (0.5 μg/kg per min)	6	5	1	0	0
Raloxifene (5 μg/kg per min)	9	8	0	0	1
Raloxifene (5 μg/kg per min) + L-NAME	7	5	0	2	0
Raloxifene (5 μg/kg per min) + CTX	7	5	1	0	1
Raloxifene (5 μg/kg per min) + L-NAME + CTX	7	5	1	1	1
L-NAME + CTX	8	6	1	1	0

CTX = charybdotoxin; L-NAME = N^G-nitro-L-arginine methyl ester; VF = ventricular fibrillation.

infarct zone. Infarct size was expressed as the percentage of the infarct zone that is contiguous with area at risk. Regional myocardial blood flow was determined by the microsphere technique (19).

Measurement of activity of MAP kinases. For the measurement of activity of MAP kinases, 0.5 g myocardial tissue was homogenized, and an in vitro kinase assay was carried out. Extracts from tissue homogenization were subjected to immunoprecipitation with anti-p38 MAP kinase antibody bound to protein A/agarose (Amersham Pharmacia Biotech, Piscataway, New Jersey), *c*-Jun fusion protein beads (Cell Signaling Technology, Beverly, Massachusetts), anti-ERK 1/2 antibody bound to protein A/agarose (Upstate Biotechnology, Waltham, Massachusetts). The immunoprecipitates were collected and washed extensively. Immunoprecipitates of anti-p38 MAP kinase and anti-ERK 1/2 antibody were mixed with 2 mg/ml dephosphorylated MAP kinase-2 activated protein and myelin basic protein (MBP), respectively, as a substrate, and 200 mmol/l adenosine triphosphate (ATP) for kinase assay. Pellets precipitated with glutathion-S-transferase/*c*-Jun/sepharose were mixed with 100 mmol/l ATP. Then, the reaction mixtures were further incubated for 30 min at 30°C. The kinase reaction was terminated by boiling in an appropriate volume of sodium dodecyl sulfate (SDS) sample buffer. The reaction components were separated by SDS/polyacrylamide gel electrophoresis and transferred to a nitrocellulose membrane. The phosphorylated MAPKAP kinase-2, *c*-Jun and MBP were detected by anti-phospho-MAPKAP kinase-2 (Upstate Biotechnology), antiphosphorylated *c*-Jun (Cell Signaling Technology), and antiphosphorylated MBP (Upstate Biotechnology) antibodies, respectively. The total content of p38 MAP kinase, *c*-Jun, or ERK in the samples was also determined by immunoblot analysis using anti-p38 MAP kinase, *c*-Jun, and ERK 1/2 antibodies. The band density was analyzed by NIH image software.

Measurement of myocardial myeloperoxidase (MPO) activity. Several myocardial tissue samples were taken from ischemic areas or nonischemic areas in each dog, frozen in liquid nitrogen and stored at −45°C until assay. The technical procedure was previously described (20). One unit of MPO activity was defined as that which degraded 1 mol hydrogen peroxide per minute at 25°C.

Statistical analysis. Data are expressed as the mean value ± SE. Statistical significance was performed with analysis of variance, and if differences were revealed among groups, they were assessed using the Fisher-Irwin test. A value of $p < 0.05$ was considered statistically significant.

RESULTS

Assignments and exclusions. The number of dogs assigned and excluded in each group is shown in Table 1.

Effects of raloxifene on infarct size. Heart rate and mean arterial blood pressure remained stable among the experimental groups throughout the study (Fig. 1). Both coronary blood flow and coronary perfusion pressure in all experimental groups did not significantly change during raloxifene infusion, although coronary blood flow in the raloxifene (5 μg/kg per min) group tended to increase at the end of raloxifene treatment, but it was not statistically significant, and the area at risk and collateral blood flow were also similar among all groups (Table 2).

The infarct size in the control group was 40.9 ± 3.9% of the area at risk, and vehicle did not have an infarct size–limiting effect (infarct size 37.4 ± 4.8%). Raloxifene (5 μg/kg per min) significantly reduced the infarct size compared with that of the control group (infarct size 7.2 ± 2.5%, $p < 0.01$), whereas a low dose of raloxifene (0.5 μg/kg per min) did not mediate the effect (infarct size 38.3 ± 2.0%). Figure 2 revealed that the infarct size–limiting effect was attenuated by either L-NAME (infarct size 21.4 ± 4.4%, $p < 0.05$ vs. control or raloxifene [5 μg/kg per min]) or CTX (infarct size 20.5 ± 5.0%, $p < 0.05$ vs. control or raloxifene [5 μg/kg per min]) and completely abolished by L-NAME + CTX (infarct size 37.7 ± 5.8%, $p < 0.05$ vs. L-NAME or CTX and $p < 0.01$ vs. raloxifene [5 μg/kg per min]). Only administration of the inhibitors L-NAME and CTX did not exaggerate the infarct size (40.5 ± 4.1%) compared with that of the control group.

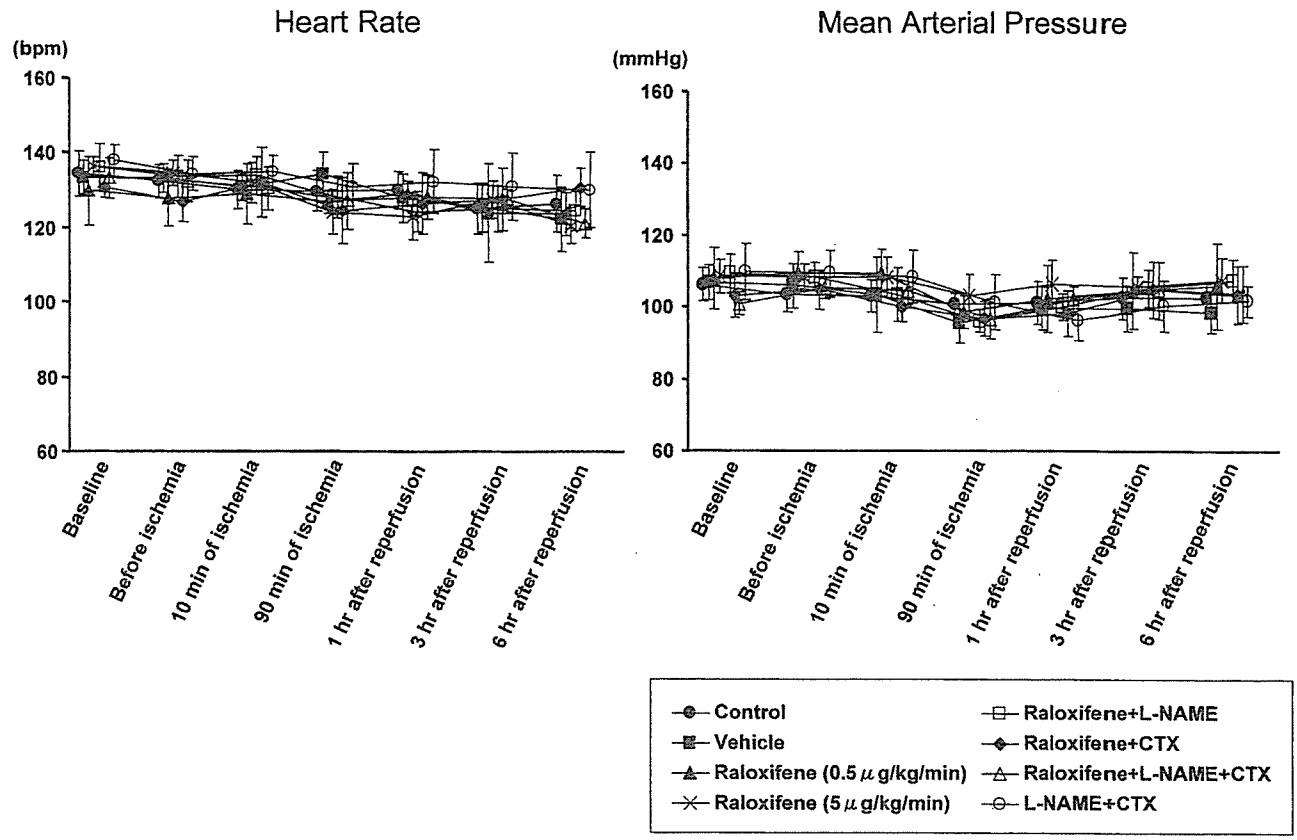

Figure 1. The changes in heart rate and mean arterial pressure during the experiment in each group are shown. No difference in heart rate or mean arterial pressure was observed throughout the experiment between the groups. CTX = charybdotoxin; L-NAME = N^G-nitro-L-arginine methyl ester.

Effects of raloxifene on VF during the reperfusion period. Pretreatment of dogs with raloxifene (5 μg/kg per min) significantly reduced the overall incidence of VF during the 6-h reperfusion period. This effect was abolished by L-NAME and CTX administered alone or together with raloxifene. At a dose of 0.5 μg/kg per min, raloxifene did not decrease the incidence of VF (Table 3).

Effects of raloxifene on MAP kinase activity during ischemia. Figure 3A shows the three major MAP kinase activities in each group, and Figure 3B demonstrates the representative results. Activities of p38 MAP kinase, JNK, and ERK in the group with ischemia were all significantly increased by 8.1 ± 1.2%, 10.4 ± 3.8% and 11.7 ± 4.9%, respectively, compared with the group with no ischemia. Activities of JNK and ERK were not different between the groups with ischemia and raloxifene pretreatment before ischemia, but only p38 activity was significantly reduced in the group with raloxifene pretreatment before ischemia, compared with the group with ischemia. Attenuation of p38 MAP kinase activity by pretreatment with raloxifene in the

Table 2. Coronary Hemodynamics, Collateral Blood Flow and Area at Risk Among Experimental Groups

Group	Before Treatment With Raloxifene		Before Ischemia		At End of Raloxifene Infusion		Collateral Blood Flow (ml/100 g per min)	Area at Risk (%)
	CPP (mm Hg)	CBF (ml/100 g per min)	CPP (mm Hg)	CBF (ml/100 g per min)	CPP (mm Hg)	CBF (ml/100 g per min)		
Control	102 ± 5	86 ± 5	104 ± 5	88 ± 6	98 ± 8	85 ± 7	10.5 ± 1.1	41 ± 3
Vehicle	105 ± 6	85 ± 6	106 ± 6	81 ± 9	105 ± 5	87 ± 13	10.2 ± 0.9	41 ± 1
Raloxifene (0.5 μg/kg per min)	107 ± 4	86 ± 6	110 ± 6	90 ± 5	100 ± 7	89 ± 11	9.3 ± 1.3	45 ± 6
Raloxifene (5 μg/kg per min)	103 ± 7	86 ± 4	108 ± 4	84 ± 9	99 ± 3	92 ± 9	10.4 ± 0.7	44 ± 2
Raloxifene (5 μg/kg per min) + L-NAME	108 ± 4	85 ± 5	108 ± 4	82 ± 9	104 ± 6	85 ± 4	10.4 ± 1.7	43 ± 1
Raloxifene (5 μg/kg per min) + CTX	105 ± 5	84 ± 5	105 ± 6	86 ± 5	104 ± 9	84 ± 6	10.1 ± 1.3	44 ± 3
Raloxifene (5 μg/kg per min) + CTX	102 ± 8	86 ± 7	105 ± 3	87 ± 5	100 ± 4	84 ± 7	9.6 ± 1.3	42 ± 1
L-NAME + CTX	106 ± 8	88 ± 9	107 ± 6	87 ± 10	101 ± 8	87 ± 9	9.4 ± 1.1	45 ± 4

Data are presented as the mean value ± SE. There was no significant difference in any value among all groups.
CBF = coronary blood flow; CPP = coronary perfusion pressure; other abbreviations as in Table 1.